7

DETECTING NUCLEAR RADIATIONS

In their basic principles of operation, most detectors of nuclear radiations follow similar characteristics: the radiation enters the detector, interacts with the atoms of the detector material (losing part or all of its energy), and releases a large number of relatively low-energy electrons from their atomic orbits. These electrons are then collected and formed into a voltage or current pulse for analysis by electronic circuitry. The choice of material to use for radiation detectors depends on the type of radiation we are trying to detect and on the information about that radiation we are trying to gather. For α particles from radioactive decays or charged particles from nuclear reactions at low (MeV) energies, very thin detectors are sufficient, as the maximum range of these particles in most solids is typically less than 100 μm. For electrons, such as those emitted in β decay, a detector of thickness 0.1 to 1 mm is required, while for γ rays the range is large and even detectors of 5-cm thickness may not be sufficient to convert energetic photons (MeV or above) into an electronic pulse. Merely to show the presence of radiation, the familiar click of the Geiger counter may be sufficient; all incident radiations give the same output. To measure the energy of the radiation, we should select a detector in which the output pulse amplitude is proportional to the energy of the radiation; here we must choose a material in which the number of released electrons is large, so that if we experience statistical fluctuations or fail to count a few, it does not substantially affect our ability to determine the energy. To determine the time at which the radiation was emitted, we must choose a material in which the electrons can be gathered quickly into the pulse; the number of electrons gathered is of considerably less importance. To determine the type of particle (such as in a nuclear reaction, in which many varieties of particles may be produced), we must choose a material in which the mass or charge of the particle gives a distinctive signature. To measure the spin or polarization of the radiation, we must choose a detector that can resolve or separate different spin or polarization states. If we expect unusually high counting rates, we must choose a detector that can recover quickly from one radiation before counting the next; for very low counting rates, we must be concerned about detecting every event and about reducing the influence of background radiations. Finally, if we are interested in reconstructing the trajectory of the detected radiations, we must have a detector that is sensitive to the location at which the radiation enters the detector.

In this chapter we discuss various types of detectors that satisfy one or another of these requirements; no single detector can satisfy all of them. We limit our discussion to radiations that are likely to be encountered in most nuclear decay and reaction studies: heavy charged particles (protons, α's) of nonrelativistic energies, relativistic electrons (of typically MeV energies), and photons in the X-ray and γ-ray regions. Neutron detectors are considered separately in Chapter 12.

7.1 INTERACTIONS OF RADIATION WITH MATTER

Heavy Charged Particles

Although Coulomb scattering of charged particles by nuclei (called Rutherford scattering) is an important process in nuclear physics, it has very little influence on the loss in energy of a charged particle as it travels through the detector material. Because the nuclei of the detector material occupy only about 10^{-15} of the volume of their atoms, it is (crudely) 10^{15} times more probable for the particle to collide with an electron than with a nucleus. The dominant mechanism for energy loss by charged particles is therefore Coulomb scattering by the atomic electrons of the detector.

Conservation of energy and momentum in a head-on elastic collision between a heavy particle of mass M and an electron of mass m (which we assume to be at rest for the sake of this simplified discussion) gives for the loss in kinetic energy of the particle

$$\Delta T = T\left(\frac{4m}{M}\right) \tag{7.1}$$

For a 5-MeV α particle (typical of those emitted in radioactive decay), this amounts to 2.7 keV. Four conclusions follow immediately:

1. It takes many thousands of such events before the particle loses all its energy. (A head-on collision gives the *maximum* energy transfer to the electron; in most collisions, the energy loss of the particle will be much smaller.)
2. In a glancing collision between an electron and a heavy particle, the heavy particle is deflected by a negligible angle, and so the particle follows very nearly a straight-line path.
3. Because the Coulomb force has infinite range, the particle interacts simultaneously with many electrons and thus loses energy gradually but continuously along its path. After traveling a certain distance, it has lost all of its energy; this distance is called the *range* of the particle. The range is determined by the type of particle, type of material, and energy of the particle. Figure 7.1 shows cloud-chamber tracks of α particles; there is a rather well-defined distance beyond which there are no particles. Usually we work with the mean range, defined so that one-half the particles have longer ranges and one-half shorter; the variation about the mean is very small, at most a few percent, so the mean range is a useful and precisely defined quantity.

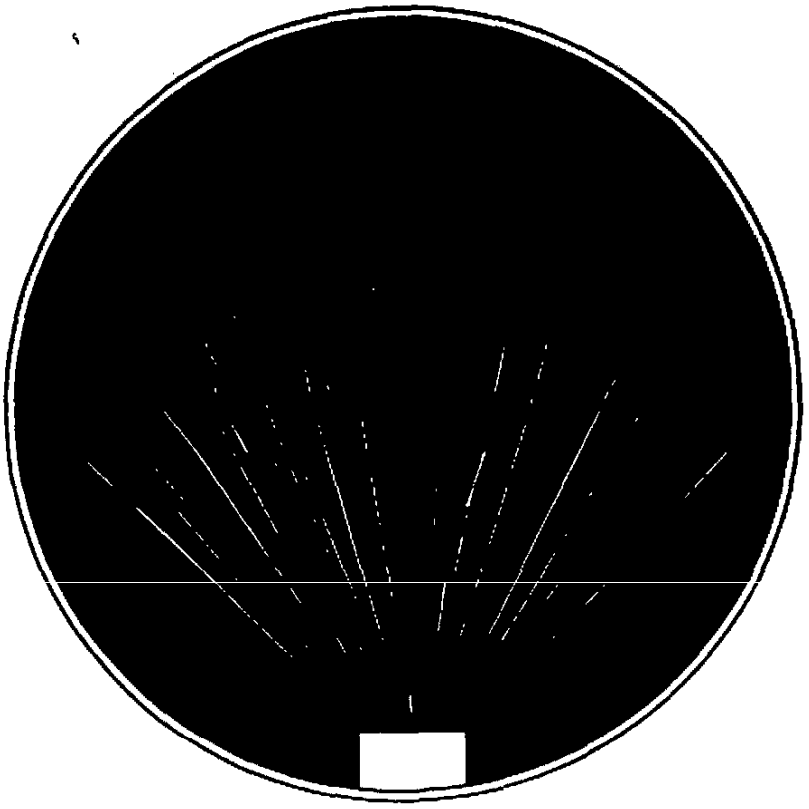

Figure 7.1 Cloud chamber tracks of α particles from the decay of ^{210}Po.

4. The energy needed to ionize an atom (i.e., to remove an electron) is of the order of 10 eV; thus many collisions will transfer enough energy to an electron to ionize the atom. (If the electron is not given enough energy to produce an ion, the atom is placed into an excited state, which quickly de-excites back to the ground state.) Furthermore, electrons given energies in the keV region (which are known as *delta* rays) can themselves produce ions by collisions, resulting in even more *secondary* electrons. To determine the energy lost by the particle, we must include the primary and secondary electrons as well as the atomic excitations.

Figure 7.2 shows the relationship between range and energy for air and for some other commonly encountered materials. For materials that are not shown, an estimate of the range can be made using a semiempirical relationship known as the Bragg-Kleeman rule:

$$\frac{R_1}{R_0} \cong \frac{\rho_0 \sqrt{A_1}}{\rho_1 \sqrt{A_0}} \tag{7.2}$$

where R is the range, ρ the density, and A the atomic weight. The subscripts 0 and 1 refer, for instance, to the known and unknown ranges and materials, respectively.

The theoretical relationship between range and energy can be obtained from a quantum mechanical calculation of the collision process, which was first done in 1930 by Hans Bethe. The calculation gives the magnitude of the energy loss per unit length (sometimes called the *stopping power*):

$$\frac{dE}{dx} = \left(\frac{e^2}{4\pi\epsilon_0}\right)^2 \frac{4\pi z^2 N_0 Z\rho}{mc^2\beta^2 A}\left[\ln\left(\frac{2mc^2\beta^2}{I}\right) - \ln(1-\beta^2) - \beta^2\right] \tag{7.3}$$

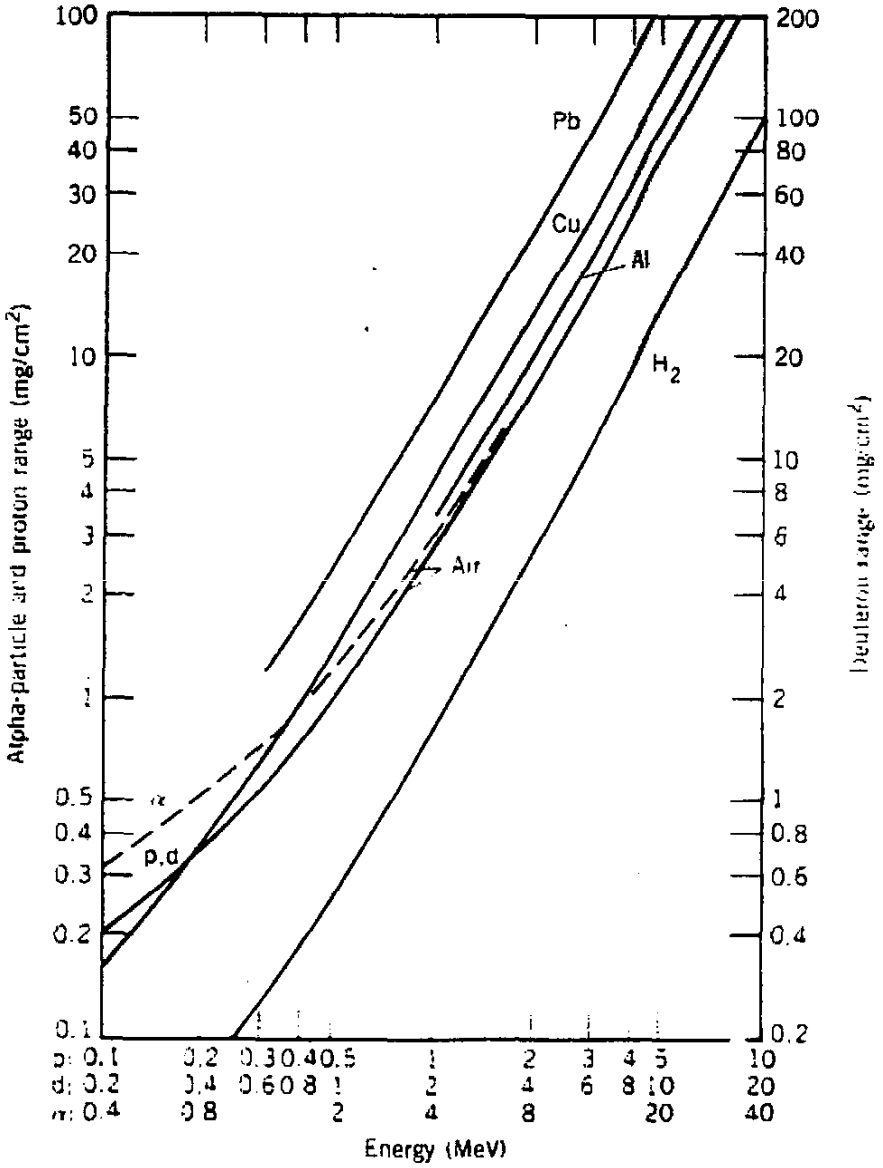

Figure 7.2 The range-energy relationship in various materials. Because the particles lose energy through scattering by atomic electrons, the range depends inversely on the density. It is therefore convenient to plot the product range × density, in units of mg/cm^2. Unfortunately, this product is also called "range" in the literature. *From* A. H. Wapstra et al., *Nuclear Spectroscopy Tables* (Amsterdam: North-Holland, 1959).

where $v = \beta c$ is the velocity of the particle, ze is its electric charge, Z, A, and ρ are the atomic number, atomic weight, and density of the stopping material, N_0 is Avogadro's number, and m is the electron mass. The parameter I represents the mean excitation energy of the atomic electrons, which could in principle be computed by averaging over all atomic ionization and excitation processes. In practice, I is regarded as an empirical constant, with a value in eV of the order of $10Z$. In air, for instance, $I = 86$ eV, while for Al, $I = 163$ eV.

The range can be calculated by integrating Equation 7.3 over the energies of the particle

$$R = \int_T^0 \left(-\frac{dE}{dx} \right)^{-1} dE \tag{7.4}$$

However, Equation 7.3 fails at low energy near the end of the range, primarily

because it does not take into account the capture of electrons by the now slow-moving particle. It is possible to write Equation 7.4 in the following form:

$$R = Mz^{-2} \int f(v)\, dv \tag{7.5}$$

where $f(v)$ is a function of the velocity of the particle that is independent of its mass and charge. We can therefore compare ranges in the same material for different particles of the same initial velocity:

$$\frac{R_1}{R_0} = \frac{M_1}{M_0} \frac{z_0^2}{z_1^2} \tag{7.6}$$

Electrons

Electrons (positive and negative) interact through Coulomb scattering from atomic electrons, just like heavy charged particles. There are, however, a number of important differences: (1) Electrons, particularly those emitted in β decay, travel at relativistic speeds. (2) Electrons will suffer large deflections in collisions with other electrons, and therefore will follow erratic paths. The range (defined as the linear distance of penetration into the material) will therefore be very different from the length of the path that the electron follows. (3) In head-on collisions of one electron with another, a large fraction of the initial energy may be transferred to the struck electron. (In fact, in electron–electron collisions we must take into account the identity of the two particles; after the collision, we cannot tell which electron was incident and which was struck.) (4) Because the electron may suffer rapid changes in the direction and the magnitude of its velocity, it is subject to large accelerations, and accelerated charged particles must radiate electromagnetic energy. Such radiation is called *bremsstrahlung* (German for "braking radiation").

The expressions for the energy loss per unit path length for electrons were also derived by Bethe, and can be written in a form similar to Equation 7.3:

$$\left(\frac{dE}{dx}\right)_c = \left(\frac{e^2}{4\pi\epsilon_0}\right)^2 \frac{2\pi N_0 Z\rho}{mc^2\beta^2 A}\left[\ln \frac{T(T+mc^2)^2\beta^2}{2I^2mc^2} + (1-\beta^2) - \left(2\sqrt{1-\beta^2} - 1 + \beta^2\right)\ln 2 + \tfrac{1}{8}\left(1-\sqrt{1-\beta^2}\right)^2\right] \tag{7.7}$$

$$\left(\frac{dE}{dx}\right)_r = \left(\frac{e^2}{4\pi\epsilon_0}\right)^2 \frac{Z^2 N_0 (T+mc^2)\rho}{137m^2c^4A}\left[4\ln\frac{2(T+mc^2)}{mc^2} - \frac{4}{3}\right] \tag{7.8}$$

where T is the kinetic energy of the electron. The subscripts c and r stand for the energy losses due to collisions and radiation, respectively. The expression for the radiative loss is valid only for relativistic energies; below 1 MeV, the radiation losses are negligible.

The total energy loss is just the sum of these two contributions:

$$\frac{dE}{dx} = \left(\frac{dE}{dx}\right)_c + \left(\frac{dE}{dx}\right)_r \tag{7.9}$$

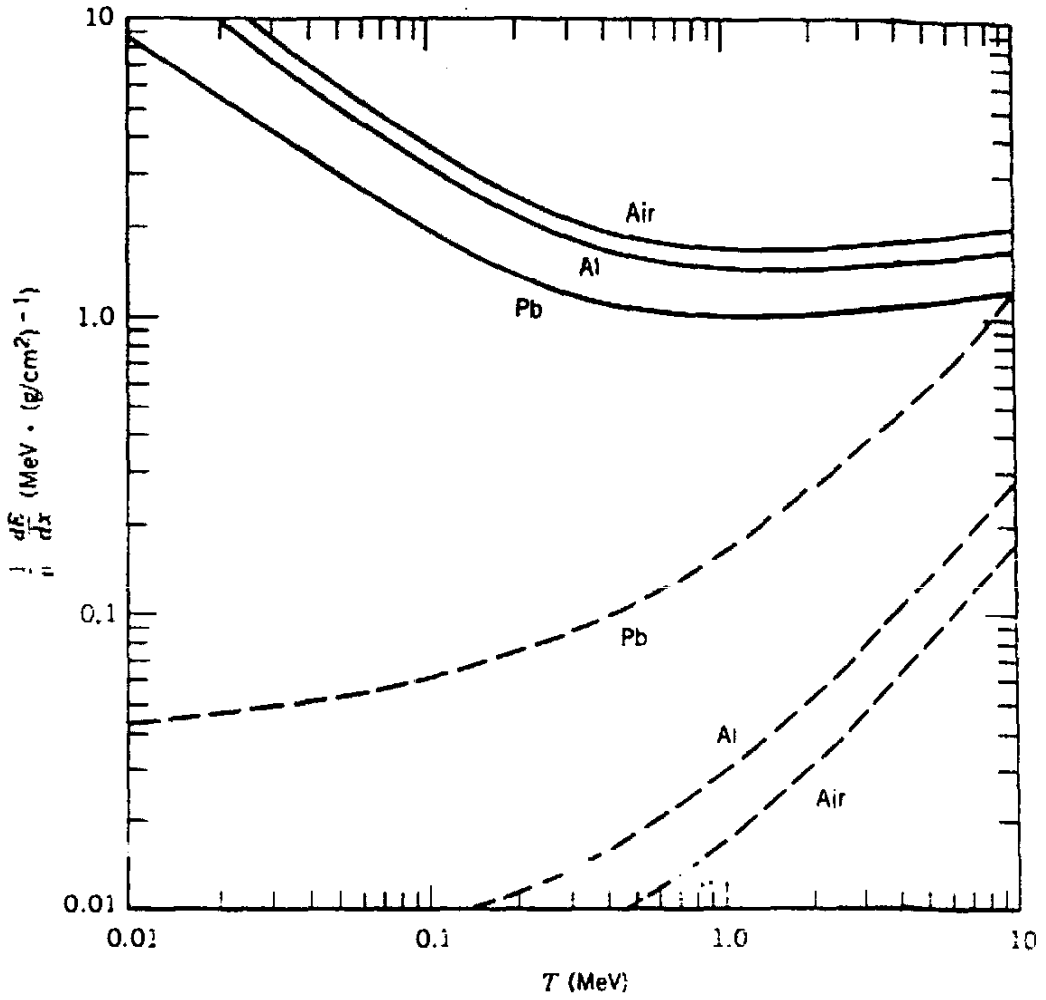

Figure 7.3 Energy loss by electrons in air, Al, and Pb. To suppress the large variation in dE/dx arising from the number of electrons of the material, the quantity $\rho^{-1}(dE/dx)$ is plotted. Solid lines are for collisions; dashed lines are for radiation. For additional tabulated data on energy losses, see L. Pages et al., *Atomic Data* **4**, 1 (1972).

To estimate the relative contributions of the two terms we can form their ratio, which in the relativistic region is approximately

$$\frac{(dE/dx)_r}{(dE/dx)_c} \approx \frac{T + mc^2}{mc^2} \frac{Z}{1600} \tag{7.10}$$

The radiative term is thus significant only at high energy and in heavy materials. Figure 7.3 shows the relative contributions for air, aluminum, and lead; for most materials used as electron detectors, the radiative contribution is small. Moreover, there is very little variation of the collisional losses with electron energy.

Calculation of the range of electrons could in principle be done by integrating Equations 7.7 and 7.8 over the path of the electrons; however, because of the random nature of the path, this is a difficult process. Instead, we use empirical data on absorption of beams of monoenergetic electrons to generate the range-energy relationship for electrons; Figure 7.4 is an example of this relationship. Based on the comparison of $\rho^{-1}(dE/dx)$ values in Figure 7.3, we conclude that the variation with type of absorber is small, and we can thus use Figure 7.4 to estimate ranges (in mg/cm^2, which is in reality range times density) in other materials as well.

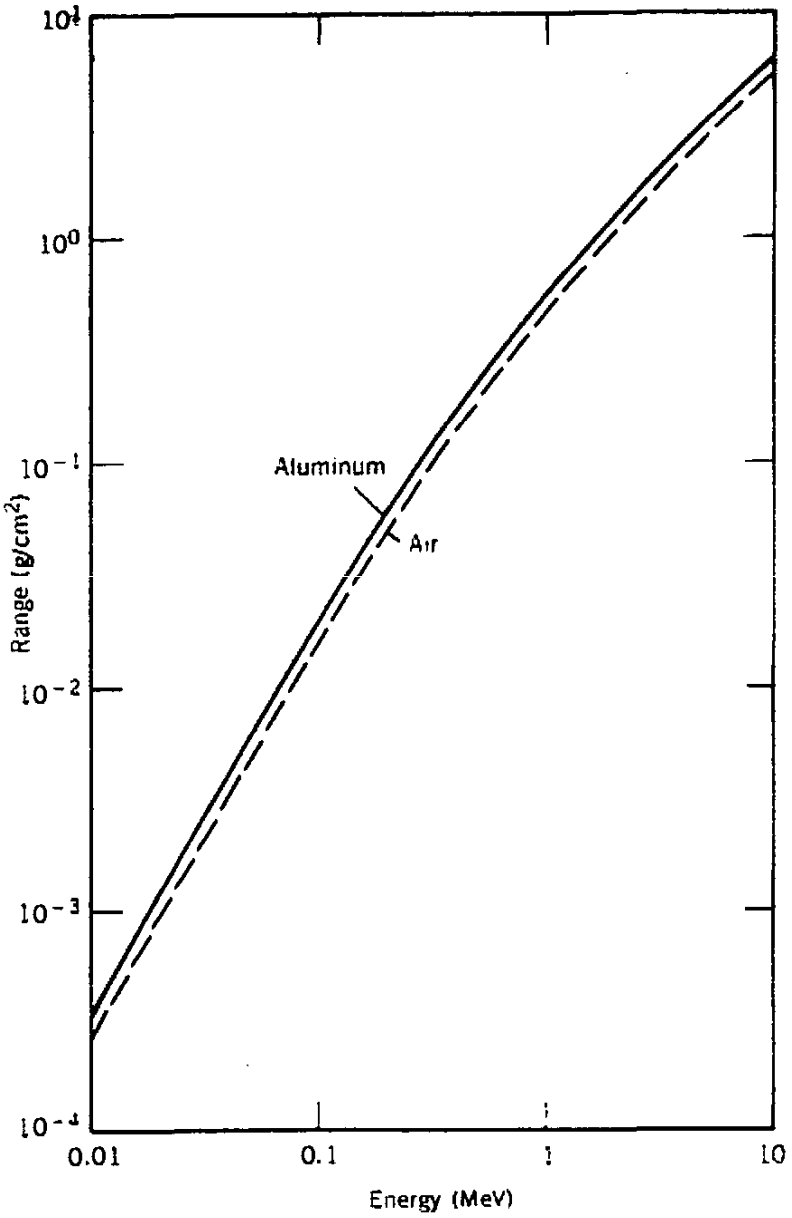

Figure 7.4 Range-energy relationship for electrons in air and in aluminum.

Electromagnetic Radiation

Gamma rays and X rays interact with matter primarily through three processes: photoelectric absorption, Compton scattering, and pair production. In the photoelectric effect, a photon is absorbed by an atom and one of the atomic electrons, known in this case as a photoelectron, is released. (Free electrons cannot absorb a photon and recoil. Energy and momentum cannot both be conserved in such a process; a heavy atom is necessary to absorb the momentum at little cost in energy.) The kinetic energy of the electron is equal to the photon energy less the binding energy of the electron:

$$T_e = E_\gamma - B_e \tag{7.11}$$

The probability for photoelectric absorption is difficult to calculate, but from experimental studies we know several features: it is most significant for low-energy photons ($\sim$ 100 keV), it increases rapidly with the atomic number Z of the absorber atoms (roughly as Z^4), and it decreases rapidly with increasing

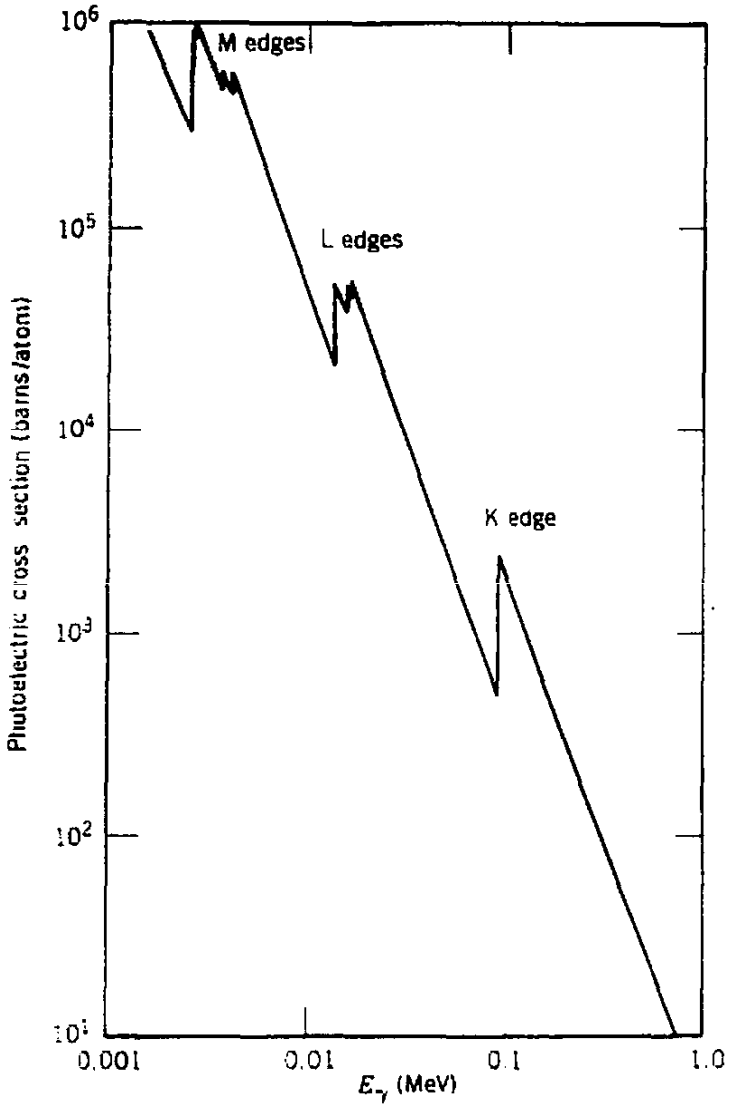

Figure 7.5 Photoelectric cross section in Pb. The discrete jumps correspond to the binding energies of various electron shells; the K-electron binding energy, for example, is 88 keV. To convert the cross section to the linear absorption coefficient τ in cm^{-1}, multiply by 0.033.

photon energy (roughly as E_γ^{-3}). Furthermore, there are in the probability for photoelectric absorption discontinuous jumps at energies corresponding to the binding energies of particular electronic shells. That is, the binding energy of a K-shell electron in Pb is 88 keV. Incident photons of energy less than 88 keV cannot release K-shell photoelectrons (although they can release less tightly bound electrons from higher shells). When the photon energy is increased above 88 keV, the availability of the K-shell electrons to participate in the photoelectric absorption process causes a sudden increase in the absorption probability, known as the K-absorption edge or simply K edge. Figure 7.5 shows a sample of the photoelectric absorption cross section.

Compton scattering is the process by which a photon scatters from a nearly free atomic electron, resulting in a less energetic photon and a scattered electron carrying the energy lost by the photon. Figure 7.6 shows a schematic view of the process. If we regard the struck electron as free and at rest (a good approximation, since the photon energy is usually large compared with the orbital energies of the loosely bound outer atomic electrons), then conservation of linear

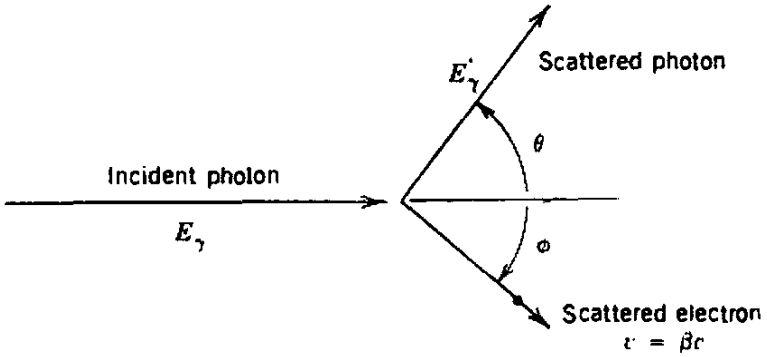

Figure 7.6 The geometry of Compton scattering.

momentum and total energy (using relativistic dynamics) gives

$$\frac{E_\gamma}{c} = \frac{E'_\gamma}{c}\cos\theta + \frac{mc\beta\cos\phi}{\sqrt{1-\beta^2}} \tag{7.12}$$

$$0 = \frac{E'_\gamma}{c}\sin\theta - \frac{mc\beta\sin\phi}{\sqrt{1-\beta^2}} \tag{7.13}$$

$$E_\gamma + mc^2 = E'_\gamma + \frac{mc^2}{\sqrt{1-\beta^2}} \tag{7.14}$$

If we observe the scattered photon, then we may eliminate the unobserved variables β and ϕ, giving the Compton-scattering formula

$$E'_\gamma = \frac{E_\gamma}{1 + (E_\gamma/mc^2)(1-\cos\theta)} \tag{7.15}$$

The scattered photons range in energy from E_γ for $\theta = 0°$ (forward scattering, corresponding to no interaction) to a minimum of roughly $mc^2/2 \approx 0.25$ MeV for $\theta = 180°$ when the photon energy is large.

The probability for Compton scattering at an angle θ can be determined through a quantum mechanical calculation of the process. The result is the *Klein-Nishina formula* for the differential cross section per electron:

$$\frac{d\sigma_c}{d\Omega} = r_0^2\left[\frac{1}{1+\alpha(1-\cos\theta)}\right]^3\left[\frac{1+\cos\theta}{2}\right] \times\left[1 + \frac{\alpha^2(1-\cos\theta)^2}{(1+\cos^2\theta)[1+\alpha(1-\cos\theta)]}\right] \tag{7.16}$$

Here α is the photon energy in units of the electron rest energy ($\alpha = E_\gamma/mc^2$) and r_0 is a parameter called the *classical electron radius*, $r_0 = e^2/4\pi\epsilon_0 mc^2 = 2.818$ fm. (This is merely a convenient parameter and has nothing whatever to do with the "size" of the electron.) Figure 7.7 shows a polar plot of the cross section.

If we are interested in the absorption of photons (that is, their removal from the incident beam of photons), we must integrate Equation 7.16 over all angles since we do not observe the scattered photon. The result is

$$\sigma_c = \frac{\pi r_0^2}{\alpha}\left\{\left[1 - \frac{2(\alpha+1)}{\alpha^2}\right]\ln(2\alpha+1) + \frac{1}{2} + \frac{4}{\alpha} - \frac{1}{2(2\alpha+1)^2}\right\} \tag{7.17}$$

for each electron in the scatterer.

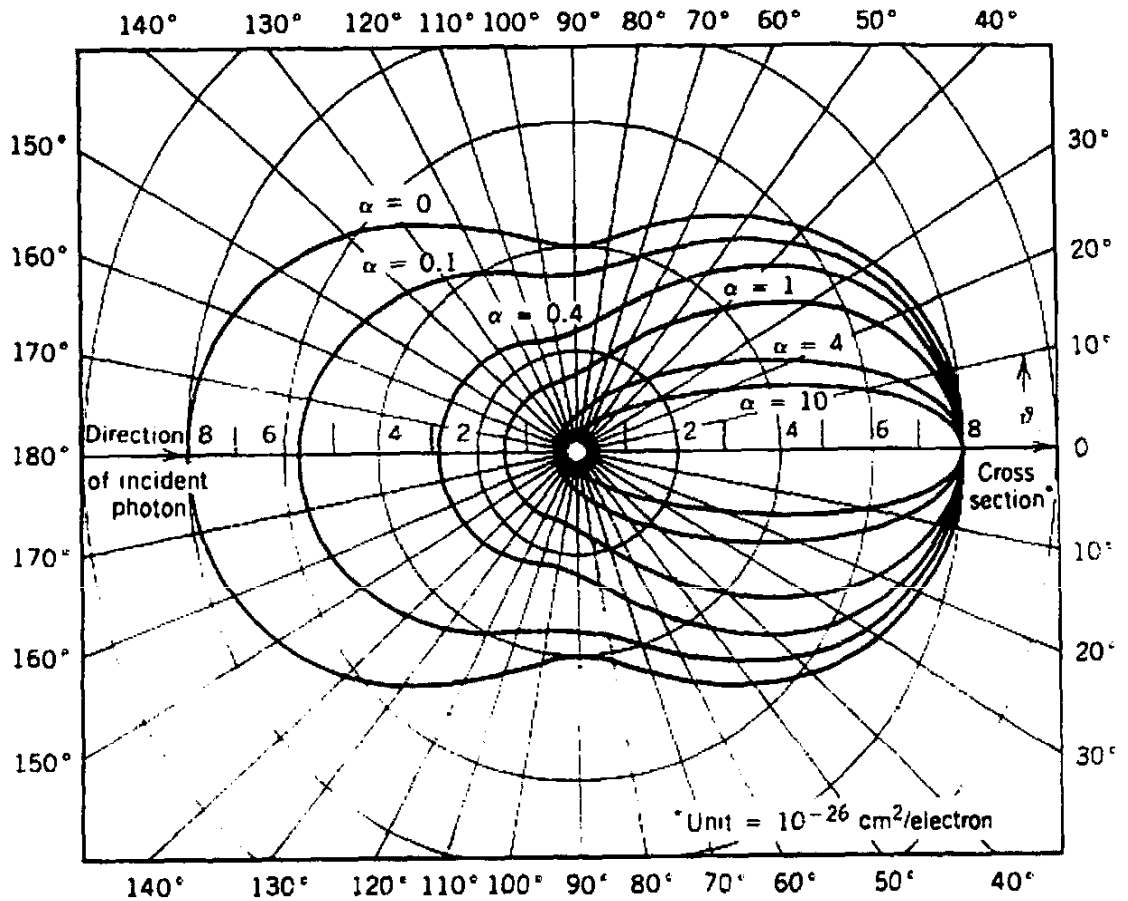

Figure 7.7 The Compton-scattering cross section for various incident energies. The polar plot shows the intensity of the scattered radiation as a function of the scattering angle θ. From R. D. Evans, *The Atomic Nucleus* (New York: McGraw-Hill, 1955).

The third interaction process is pair production, in which a photon creates an electron-positron pair; the photon disappears in this process. The energy balance is

$$E_\gamma = T_+ + mc^2 + T_- + mc^2 \tag{7.18}$$

where T_+ and T_- are the energies of the positron and electron. Like photoelectric absorption, this process requires the nearby presence of a massive atom for momentum conservation, but the recoil energy given to the atom is negligible compared with the other terms of Equation 7.18.

There is obviously a threshold of $2mc^2$, or 1.022 MeV, for this process, and in general pair production is important only for photons of high energy. Figure 7.8 shows the importance of pair production relative to the other two processes; pair production becomes dominant only for energies above 5 MeV.

Let us consider a highly collimated beam of monoenergetic photons incident on a slab of material of thickness t (Figure 7.9). The photon may undergo photoelectric absorption or pair production and thus disappear, or Compton scattering and be deflected from reaching the detector. Those photons that reach the detector are those that have no interactions at all; there are simply fewer of them than there were in the incident beam. (Contrast this situation with the case of heavy charged particles, where if t is less than the range, the number is unchanged but the energy is decreased.) The total probability *per unit length* μ for removal of a photon is called the *total linear attenuation coefficient*; it is simply the sum of the respective probabilities for photoelectric absorption (τ),

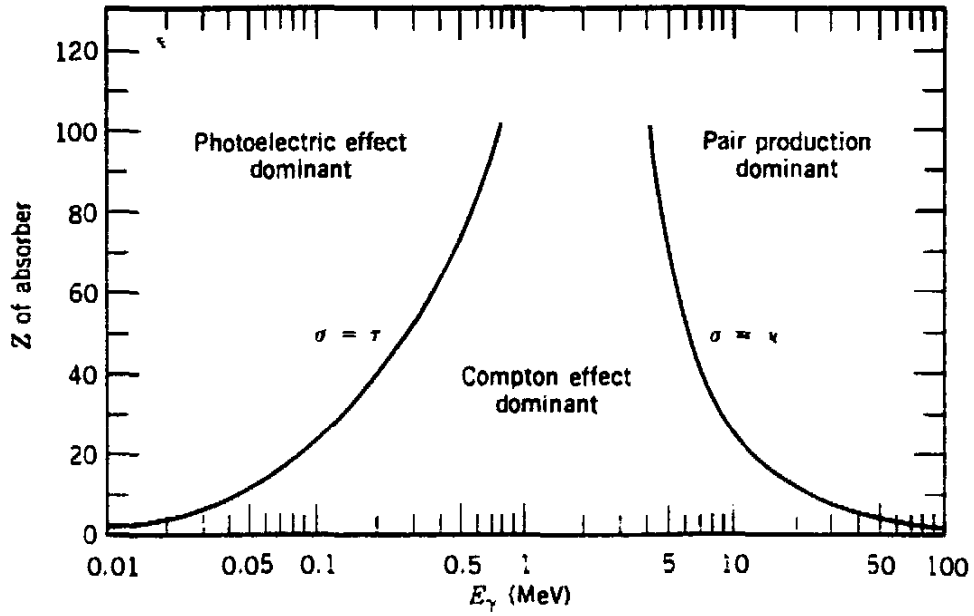

Figure 7.8 The three γ-ray interaction processes and their regions of dominance.

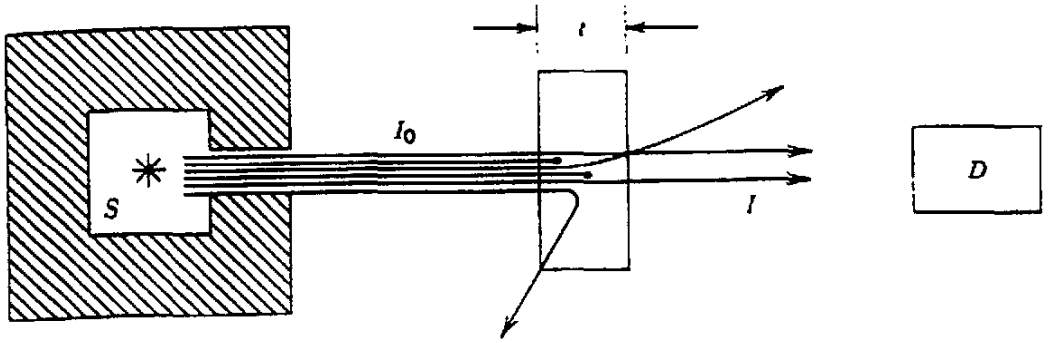

Figure 7.9 An experiment to measure absorption of radiation in a slab of material of thickness t. A beam of radiation from the source S is collimated and then is scattered or absorbed by the material. The remaining intensity I reaches the detector D.

Compton scattering (σ), and pair production (κ):

$$\mu = \tau + \sigma + \kappa \tag{7.19}$$

The linear Compton absorption coefficient σ is related to the calculated cross section per electron, σ_c of Equation 7.17, according to

$$\sigma = \sigma_c NZ \tag{7.20}$$

where Z and N again represent the atomic number of the scattering material and the number of atoms per unit volume. All quantities in Equation 7.19 have dimensions of $(\text{length})^{-1}$.

The fractional loss in intensity in crossing any thickness dx of material is

$$\frac{dI}{I} = -\mu\, dx \tag{7.21}$$

and thus

$$I = I_0 e^{-\mu t} \tag{7.22}$$

in passing through a thickness t.

Figure 7.10 shows some representative values for the energy dependence of the attenuation coefficients.

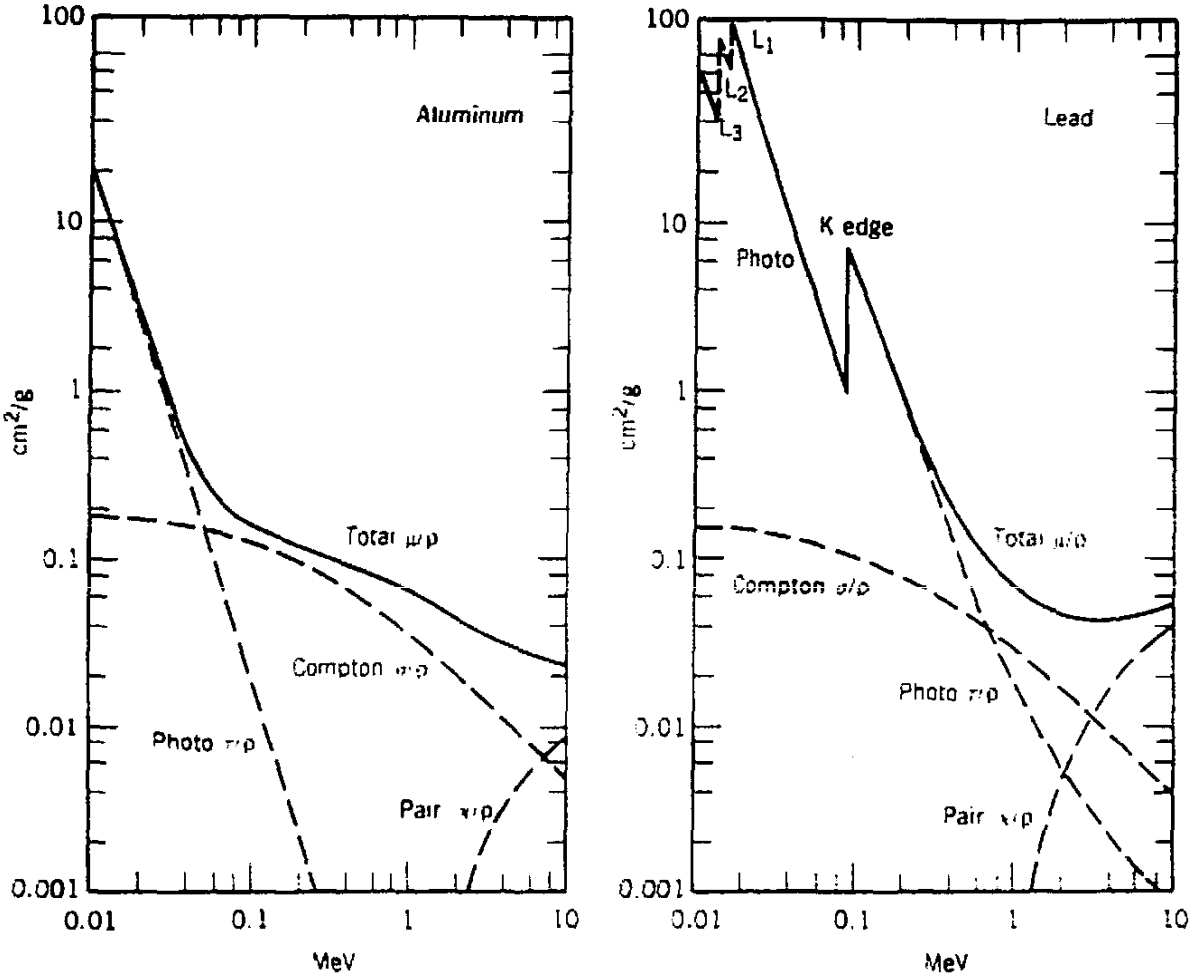

Figure 7.10 Photon mass attenuation coefficients, equal to the linear attenuation coefficients divided by the density (to suppress effects due simply to the number of electrons in the material) for the three processes in Al and Pb.

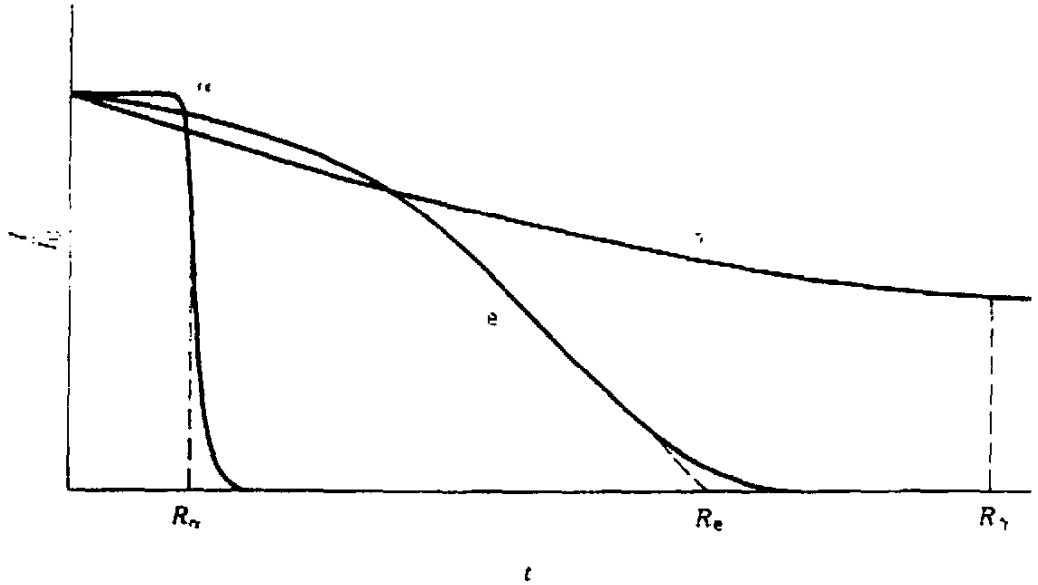

Figure 7.11 The transmitted intensity measured in a geometry such as that shown in Figure 7.9. For α's, the value of t such that $I / I_0 = 0.5$ is the mean range; for photons, with their simple exponential dependence, we can define the mean range similarly. For electrons, it is customary to define the *extrapolated* range by extending the linear portion of the absorption curve as shown. The horizontal scale is not at all linear; the range for γ's may be 10^4 that for α's.

If we were to study the loss in intensity of monoenergetic beams of 1-MeV α's, electrons, and γ radiations in a geometry such as that shown in Figure 7.9, the results might look somewhat like Figure 7.11. The α intensity is undiminished until the thickness is very close to the mean range, and then drops very quickly to zero; the range of 1-MeV α's in aluminum is about 0.0003 cm. The electron intensity begins to decrease slowly even for thicknesses much less than the range, owing to electrons that are scattered out of the beam. The extrapolated range for electrons is about 0.18 cm. The γ intensity decreases exponentially; the mean range (defined as the thickness such that $I = 0.5I_0$) is about 4.3 cm for a 1-MeV γ in aluminum.

Note the somewhat different uses of the concept of range in these cases, and be sure to note that for α's and β's but not for γ's the energy per particle observed in the geometry of Figure 7.9 would decrease as the beam traveled through the material.

7.2 GAS-FILLED COUNTERS

The function of many detectors of nuclear radiation is to use an electric field to separate and count the ions (or electrons) formed as a result of the passage of radiation through the detector. The simplest type of detector that accomplishes this is the *ionization chamber*, which we can regard as a parallel-plate capacitor in which the region between the plates is filled with a gas, often air. The electric field in this region keeps the ions from recombining with the electrons, and it is useful to picture a cloud of electrons drifting toward the plate held at positive potential, while the positively charged ions drift toward the other plate. In air, the average energy needed to produce an ion is about 34 eV; thus a 1-MeV radiation produces a maximum of about 3×10^4 ions and electrons. For a medium-sized chamber, say 10×10 cm with a plate separation of 1 cm, the capacitance is 8.9×10^{-12} F and the resulting voltage pulse is about

$$\frac{(3 \times 10^4 \text{ ions})(1.6 \times 10^{-19} \text{ C/ion})}{8.9 \times 10^{-12} \text{ F}} \cong 0.5 \text{ mV}$$

This is a rather small signal, which must be considerably amplified (by a factor of roughly 10^4) before we can analyze it using standard electronics.

The amplitude of the signal is proportional to the number of ions formed (and thus to the energy deposited by the radiation), and is independent of the voltage between the plates. The applied voltage does determine the speed at which the electron and ion clouds drift to their respective electrodes. For a typical voltage of roughly 100 V, the ions move at speeds of about 1 m/s and will take roughly 0.01 s to travel across the 1-cm chamber. (Electrons are more mobile and travel about 1000 times faster.) This is an exceedingly long time by standards of nuclear counting (a weak radioactive source of 1 μCi activity gives on the average one decay every 30 μs), and thus the ion chamber is of no use in counting individual pulses. It does find wide use as a radiation monitor, and many commercial radiation monitors are in fact ion chambers. The radiation intensity is recorded as a *current* representing the interaction of many radiations during the response time of the chamber. The current output is proportional both to the activity of

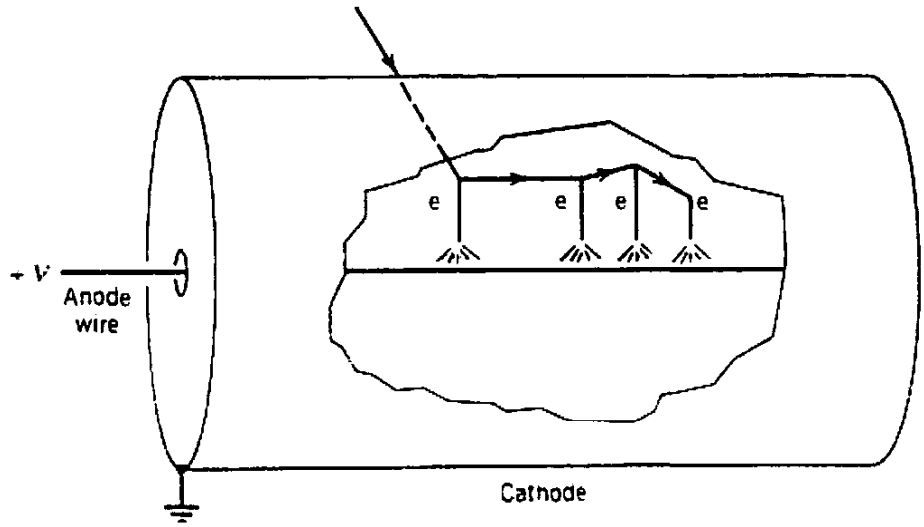

Figure 7.12 The geometry of a cylindrical proportional counter. The incoming radiation creates many electron-ion pairs. The electrons drift relatively slowly until they reach the neighborhood of the anode wire, where they are accelerated rapidly and create many secondary ionizations.

the source and to the energy of the radiations—higher energy radiations give more ionization and thus a greater response.

To use a gas-filled detector to observe individual pulses, we must provide considerable amplification. One way of accomplishing this is to increase the voltage to larger values, usually in excess of 1000 V. The larger electric field is able to accelerate the electrons that result from the ionization process; rather than drifting slowly toward the anode, making occasional elastic collisions with gas atoms, the accelerated electrons can acquire enough energy to make inelastic collisions and even to create new ionized atoms (and more electrons to be accelerated in turn). This rapid amplification through production of *secondary* ionizations is called a *Townsend avalanche*. Even though there is a large number (perhaps 10^3–10^5) of secondary events for each original ion, the chamber is always operated such that the number of secondary events is proportional to the number of primary events, and the device is therefore known as a *proportional counter*.

The geometry of the proportional counter is usually cylindrical, as shown in Figure 7.12. The electric field in this geometry at a radius r is

$$E(r) = \frac{V}{r \ln(b/a)} \tag{7.23}$$

where b is the inner radius of the cathode and a is the outer radius of the anode wire. The avalanche will obviously occur in the high-field region near the anode wire. This region, however, represents only a very small fraction of the volume of the chamber. The vast majority of the original ions are formed far from this central region, and the electrons drift slowly until they begin the avalanche process. (A primary event that occurs within the high-field region would experience a somewhat smaller amplification factor because it would not have the opportunity to make as many collisions.)

Because the output signal of a proportional counter comes mainly from the avalanche process, which occurs very rapidly, the timing is determined by the

drift time of the primary electrons from the point of the original ion formation to the vicinity of the anode wire where the avalanche occurs. This time is of the order of microseconds, and thus the counter can be operated in a pulse mode at counting rates of the order of 10^6/s.

If the electric field is increased to even larger values, *secondary avalanches* can occur. These can be triggered by photons emitted by atoms excited in the original (or in a subsequent) avalanche. These photons can travel relatively far from the region of the original avalanche, and soon the entire tube is participating in the process. The amplification factor is perhaps as large as 10^{10}. Because the entire tube participates for every incident event, there is no information at all on the energy of the original radiation—all incident radiations produce identical output pulses. This region of operation is called the *Geiger-Müller region* and counters based on this principle are usually known as *Geiger counters*. Geiger counters also are popular as portable radiation monitoring instruments.

The output signal from a Geiger counter consists of the collected electrons from the many avalanche processes; the signal is of the order of 1 V, so no further amplification is usually required. The collection time is of the order of 10^{-6} s, during which time the positive ions do not move far from the avalanche region. There is thus surrounding the anode wire a positively charged ion cloud that reduces the electric field intensity and eventually terminates the avalanche process.

The cycle would then be completed after the positive ions have drifted to the cathode and become neutralized (which takes 10^{-4}–10^{-3} s), but during their travel they can be accelerated and strike the cathode with enough energy to release electrons (from the cathode) and to begin the process again (and because of the nature of the multiple avalanche process in the Geiger tube, all it takes is *one electron* to create an output pulse). To prevent this from occurring, a second type of gas, called the *quenching* gas, is added to the tube. The quenching gas is usually one with complex organic molecules such as ethanol; the primary gas is generally one with simple molecules, such as argon, and a typical mixture might be 90% argon and 10% ethanol. As the space charge, consisting mostly of argon ions, begins to drift toward the cathode, collisions will occur with the quenching gas in which there is a high probability of the transfer of an electron, so that the argon is neutralized and the ionized ethanol begins to drift toward the cathode. When it arrives there and is neutralized, the energy that formerly went into releasing a free electron can now be absorbed in the dissociation of the molecule (a process not possible for a simple argon atom). The quenching gas is thus gradually used up, and the Geiger tube must periodically be replaced. Other Geiger tube designs use halogens as the quenching gas; the subsequent recombination of the dissociated molecule eliminates the need to replace the tube.

The various regions of operation of gas-filled counters are summarized in Figure 7.13. For low applied voltages, recombination of the primary electrons and ions occurs. As V is increased, we reach the ion chamber region, where the pulse output is proportional to the primary ionization produced by the radiation and thus to its energy, but is independent of V. In the proportional region, the pulse amplitude rises with V to make analysis easier, but the output pulse is still proportional to the energy of the radiation through the ionization produced. Finally, the Geiger plateau is reached, where all radiations give the same output

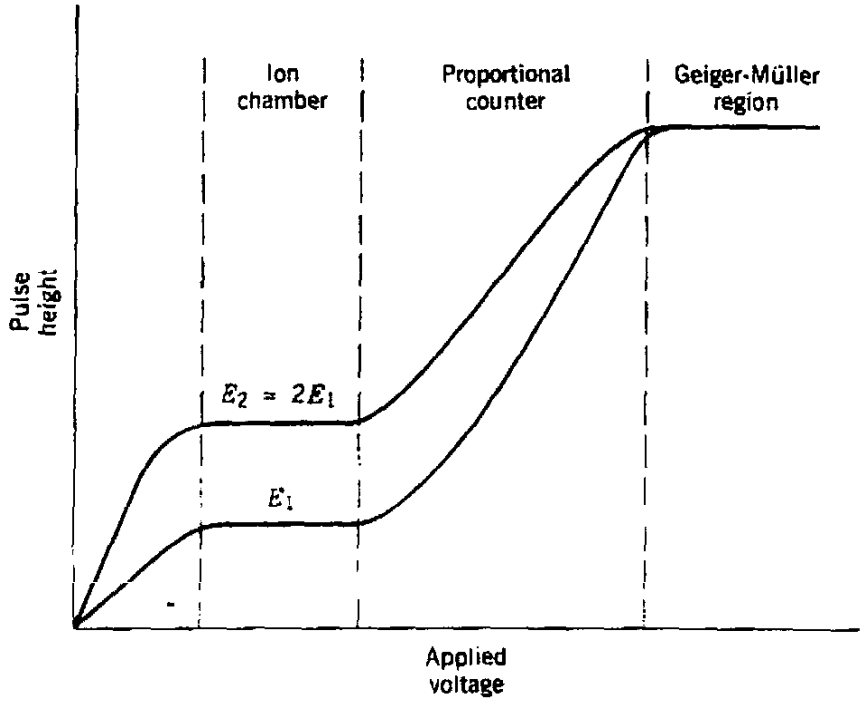

Figure 7.13 The pulse heights produced by different gas-filled counters as a function of the applied voltage, for two radiations differing in energy by a factor of 2. In the Geiger-Müller region, all radiations give the same output pulse height; in the other regions, the output pulse height is proportional to the energy deposited by the radiation through primary ionization.

pulse, irrespective of the amount of initial ionization or the energy of the radiation.

7.3 SCINTILLATION DETECTORS

A disadvantage of gas-filled counters is their low efficiency for many radiations of interest in nuclear physics—the range in air of a 1-MeV γ ray is of the order of 100 m. Solid detectors have the higher densities that give reasonable absorption probabilities for detectors of reasonable size. To make a workable solid detector, however, we must satisfy two contradictory criteria: (1) The material must be able to support a large electric field, so that the electrons and ions can be collected and formed into an electronic pulse, and little or no current must flow in the absence of radiation, so that the background noise is low. (2) Electrons must be easily removed from atoms in large numbers by the radiation, and the electrons and ionized atoms must be able to travel easily through the material. (Actually, the ions themselves do not move in a solid; instead, the electronic vacancy or "hole" is filled by successive electron transfers from one atom to the next, so that the "hole" appears to travel.) The first condition supports the choice of an insulating material, while the second suggests using a conductor. The obvious compromise is a semiconductor, and we consider such devices in the next section. Bulk semiconducting materials in sizes large enough to make useful radiation detectors (tens of cm^3) did not become available until the late 1960s, and to fill the need for nuclear spectroscopic devices of high efficiency and reasonable resolution, *scintillation counters* were developed during the 1950s.

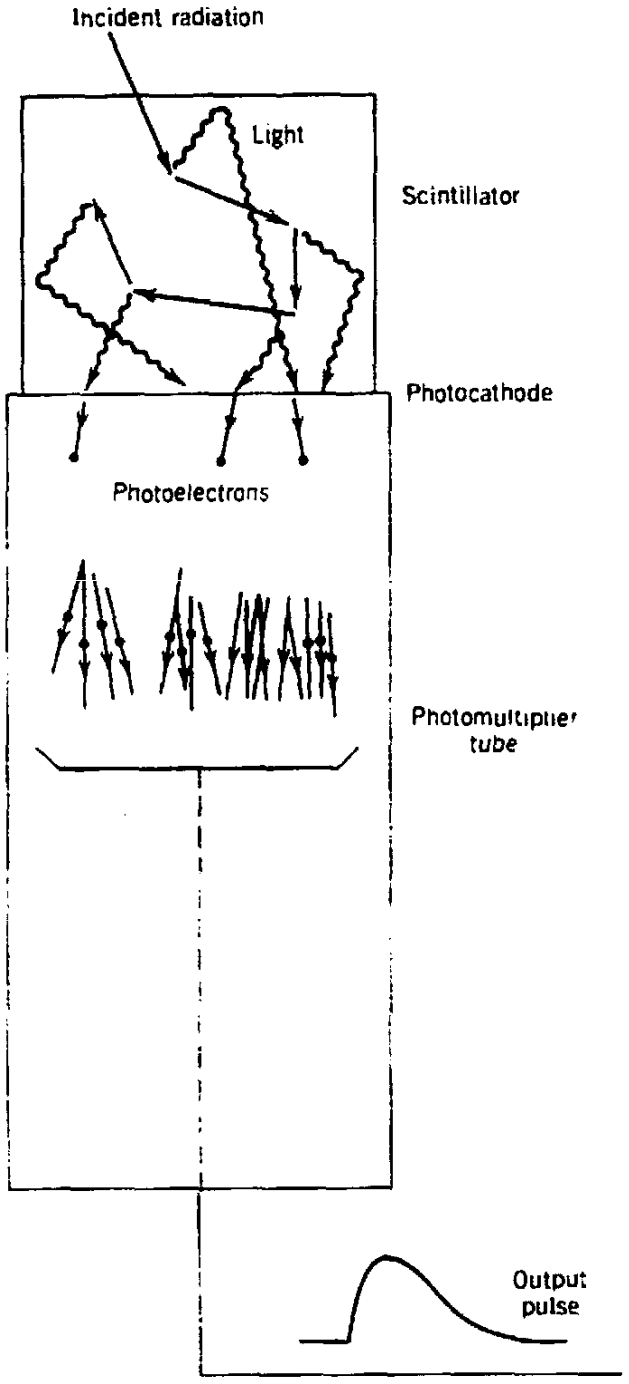

Figure 7.14 The basic processes in a scintillation detector.

Scintillation counters solve our dilemma over the choice of materials in a clever way: The electrons that are formed in the ionization process are not the same electrons that form the electronic pulse. The intermediary between the ionization electrons and the pulse electrons is ordinary light. The complete process can be understood as follows, with reference to Figure 7.14: (1) The incident radiation enters the detector and suffers a large number of interactions, which result in the raising of the atoms to excited states. (2) The excited states rapidly emit visible (or near-visible) light; the material is said to *fluoresce*. (3) The light strikes a photosensitive surface, releasing at most one photoelectron per photon. (4) These secondary electrons are then multiplied, accelerated, and formed into the output pulse in the *photomultiplier* (PM) tube.

Many different varieties of scintillators and PM tubes are available, depending on the application in which they will be used. Properties that are usually

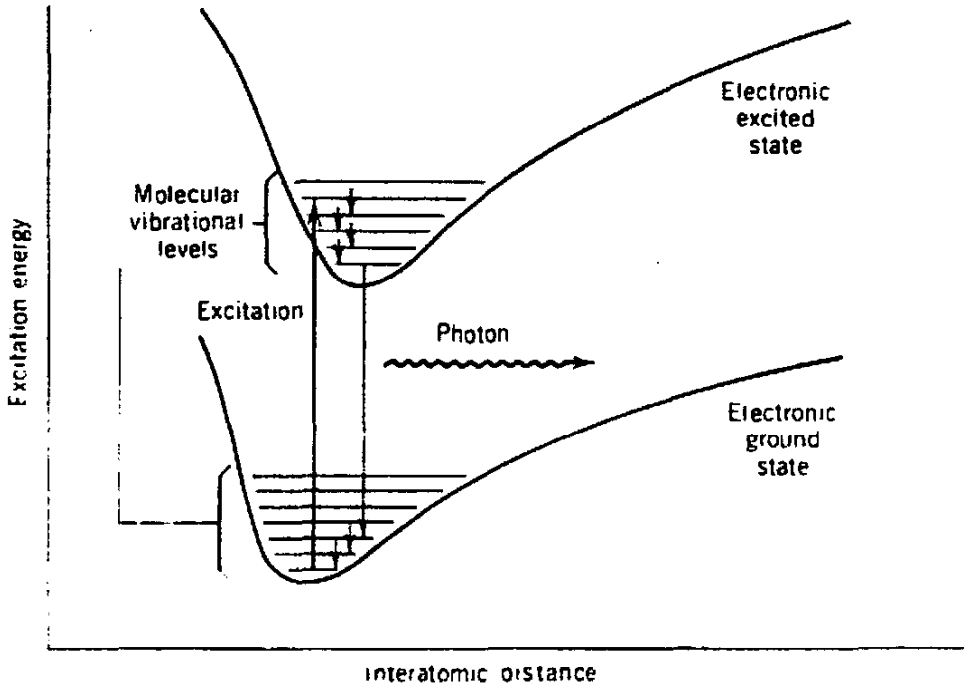

Figure 7.15 Electronic structure in an organic scintillator. The electronic states are represented as a potential minimum, resulting from the combined effects of the molecular attraction that keeps us from separating the atoms to greater distances and the repulsion that keeps us from forcing the atoms closer together (because the Pauli principle does not let the atomic wave functions overlap). Inside the electronic potential minimum is a sequence of levels that result from the atoms of the molecule vibrating against one another.

considered in making the choice of a material include light output (the fraction of the incident energy that appears as light), efficiency (the probability for the radiation to be absorbed), timing, and energy resolution. Other criteria may have to do with ease of working with the material: one common scintillator, crystalline NaI, is hygroscopic: exposure to water vapor causes a transparent crystal to become an opaque powder, and NaI must be kept sealed. On the other hand, many plastic scintillators can be cut with an ordinary saw and formed into any desired size and shape.

To understand the operation of a scintillator, we must consider the mechanisms by which energy can be absorbed in raising electrons to excited states. There are two basic types of detectors, those composed of organic materials and those composed of inorganic materials.

In organic scintillators (which can be liquid or solid), the interactions between the molecules are relatively weak, and we can discuss their properties in terms of the discrete excited states of the molecules. There are two ways in which a molecule can absorb energy: the electrons can be excited to higher excited states, and the atoms in the molecule can vibrate against one another. Typical spacing of vibrational energies is about 0.1 eV, while the electronic excitation energies are of the order of a few eV. The resulting structure may look something like that of Figure 7.15. The excited electrons are generally those not strongly involved in the bonding of the material. In aromatic hydrocarbons, such as those typified by the ring structure of benzene, three of the four valence electrons of carbon are in the hybridized orbitals called σ orbitals; these are strongly localized between each carbon, its two carbon neighbors, and a single hydrogen. The fourth

electron, which is in the so-called π orbital, is not as well localized and does not participate in the bonding process as strongly as the σ electrons. It is this π electron that is most responsible for the scintillation process.

The incoming radiation interacts with many molecules, losing a few eV at each interaction as it excites the molecule. Many possible vibrational states can be excited (and also many possible electronic excited states; for simplicity only the lowest electronic excited state is shown). These decay quickly ($\sim$ 1 ps) to the lowest vibrational state of the electronic excited state, which then decays (in a time of order 10 ns) to one of the vibrational states of the electronic ground state. These in turn decay quickly to the vibrational ground state.

Under normal circumstances, at room temperature all of the molecules of the scintillator are in the lowest vibrational state of the electronic ground state. The thermal energy kT at room temperature is 0.025 eV, and thus according to the Boltzmann population distribution $e^{-E/kT}$, it is unlikely to find any population of the vibrational states above the electronic ground state. Thus only one of the many emitted photon transitions has any probability to be absorbed. This represents an important property of a scintillator: *it must be transparent to its own radiation*.

Of the inorganic scintillators, the most common variety is the single crystal of an alkali halide; NaI is the most frequently used. A single crystal is needed to obtain transparency; reflections and absorption at the crystal faces would make a polycrystalline scintillator useless. The cooperative interactions of the atoms in a crystal cause the discrete energy levels to "smear out" into a series of energy bands. The two highest bands are the *valence band* and the *conduction band* (Figure 7.16). In an insulating material such as NaI, the valence-band states are generally full and the conduction-band states are empty. An incoming radiation can excite an electron across the *energy gap* (about 4 eV) and into the conduction band; eventually, it loses energy by emission of a photon and drops back into the valence band.

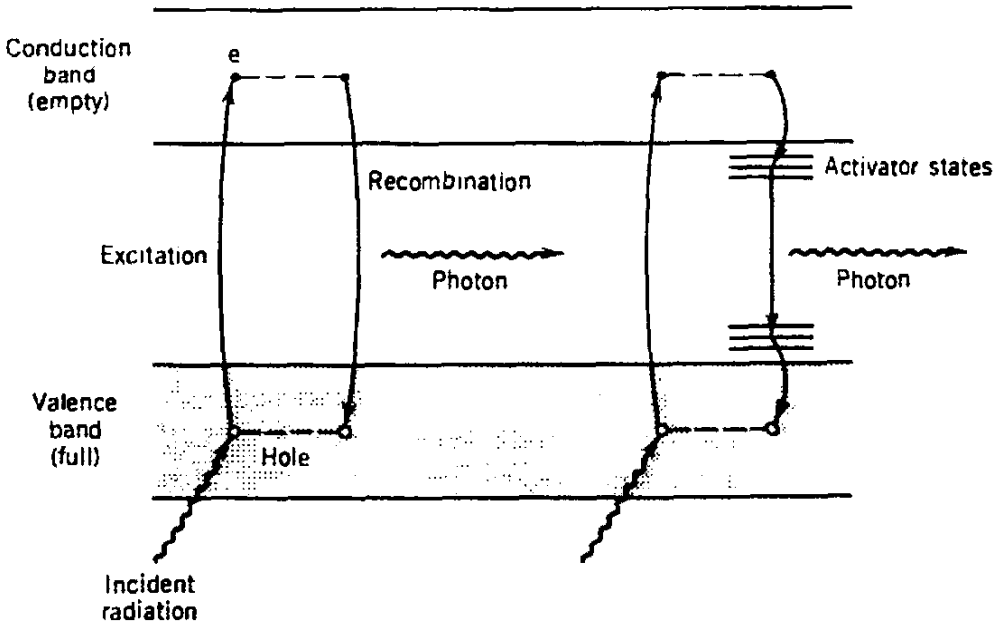

Figure 7.16 Energy bands in a crystal. At the left are shown processes characteristic of a pure crystal such as NaI. At the right are shown the processes in the presence of an activator, such as Tl in NaI(Tl).

Table 7.1 Properties of Some Common Scintillators

Name	Type	Density (g/cm^3)	Index of Refraction	Wavelength of Maximum Emission (nm)	Relative Output[a]	Time Constant (ns)
Anthracene	Organic solid	1.25	1.62	447	0.43	30
Pilot B	Plastic (organic solid)	1.03	1.58	408	0.30	1.8
NE 213	Organic liquid	0.87	1.508	425	0.34	3.7
NaI(Tl)	Inorganic crystal	3.67	1.85	410	1.00	230
CsF	Inorganic crystal	4.11	1.48	390	0.05	5

[a] The relative output includes the typical efficiency for photon absorption and the resulting light output.

To increase the probability for photon emission and to reduce self-absorption of the light, small amounts of impurities called *activators* are added to the crystal. A commonly used activator is thallium, and so these detectors are indicated as, for instance, NaI(Tl). The activator provides states in the energy gap and the light emission takes place between the activator states. In the case of NaI, the wavelength of maximum emission is shifted from 303 nm in pure NaI to 410 nm in NaI(Tl). Absorption at this energy cannot occur in NaI(Tl), because the activator ground states are not populated, and the change in wavelength from the ultraviolet to the visible gives a better overlap with the maximum sensitivity of most photomultiplier tubes.

Table 7.1 shows some properties of some commonly used scintillation detectors. The actual choice of scintillator will depend on the type of experiment that is being done. For example, where high efficiency for γ rays is concerned,

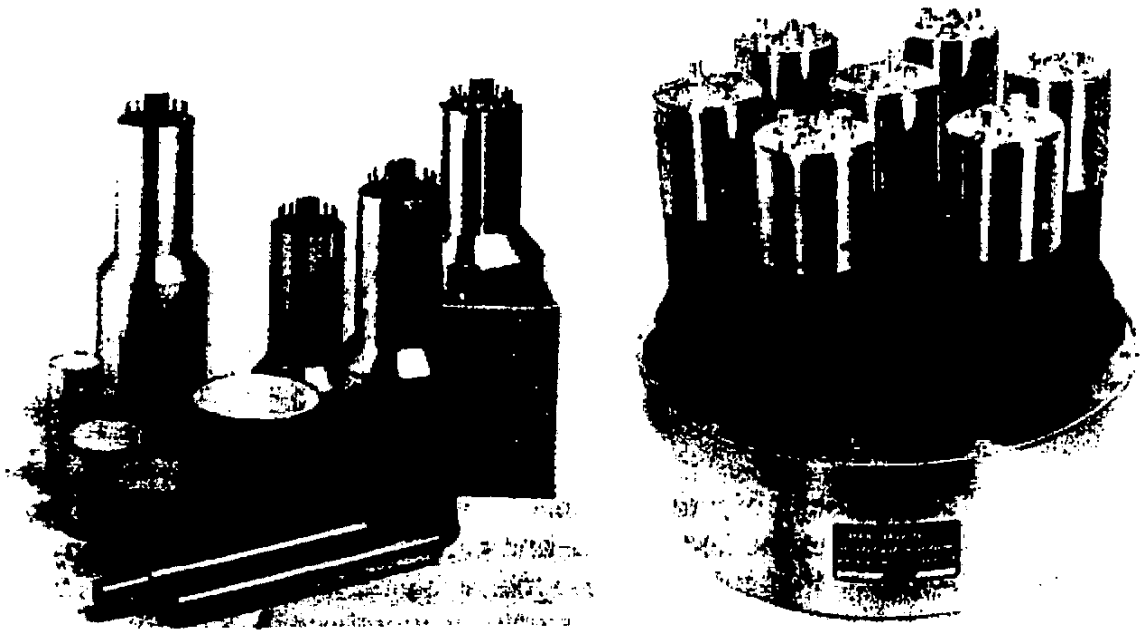

Figure 7.17 (Left) A selection of NaI scintillators, some with photomultiplier tubes attached. (Right) A large NaI detector viewed by seven photomultipliers. Reproduced with permission of Harshaw / Filtrol Partnership.

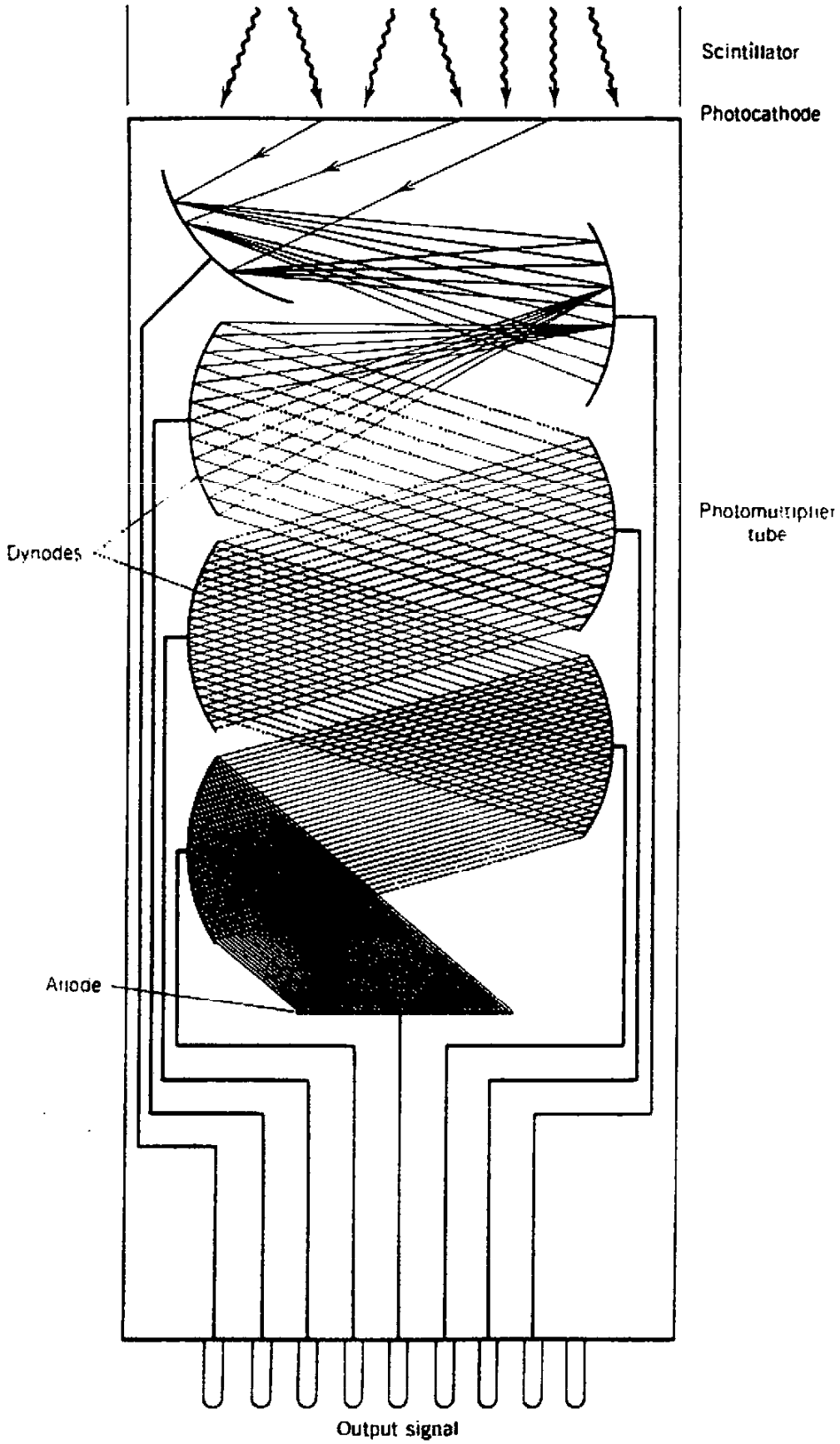

Figure 7.18 Schematic of photomultiplier operation. Electrons released from the cathode are attracted to the first dynode and multiplied. Each successive dynode is at a higher potential that the previous one; a typical tube might have 10 or 14 dynodes. At each stage, the number of electrons increases by a factor of the order of 5.

NaI(Tl) is usually the choice, the large Z (53) of I giving a high probability for photon absorption. However, for precise timing, NaI(Tl) is not very good and the relatively less efficient plastic scintillator may be a better choice.

The coupling of a scintillator to a photomultiplier tube can be done in a variety of ways. Some detector-tube combinations are purchased as a sealed unit. NaI(Tl) detectors can be placed into direct contact with the glass of the PM tube using transparent "optical grease" to provide a relatively uniform change in index of refraction and minimize internal reflection. Sometimes the photomultiplier geometry is very different from the scintillator geometry or it must be located far away from the scintillator (to eliminate the effects of magnetic fields, for instance). In this case a "light pipe" is used; light pipes can be cut to any size or shape out of any ordinary transparent material such as Lucite. Both the scintillator and the light pipe must be wrapped with reflective material to improve the efficiency of light collection. Figure 7.17 shows a selection of scintillation detectors, light pipes, and PM tubes.

A schematic diagram of a PM tube is shown in Figure 7.18. A small number of electrons (smaller than the number of incident photons) is released at the photocathode, then multiplied and focused by a series of electrodes called *dynodes*. The dynodes are connected to a voltage chain produced by a high-voltage supply and a series of voltage dividers. The typical potential difference between adjacent dynodes is about 100 V, and thus electrons strike the dynodes with about 100 eV of energy. The dynodes are constructed of materials with a high probability of secondary electron emission: it may take 2–3 eV to release an electron and thus a gain in the number of electrons of factors of 30–50 is possible. However, because the electrons are released in random directions in the material, relatively few will actually be released at the surface, and a gain of 5 at each dynode is more typical. Even so, with a 10-dynode tube, the overall gain would be 5^{10} (about 10^7). For energy spectrometers, two important characteristics are *linearity* and *stability*. Linearity means that the amplitude of the eventual output pulse must be directly proportional to the original number of scintillation events and thus in turn to the energy deposited in the detector by the radiation. Because the gain of each dynode stage depends on the voltage difference, any change in the high voltage will cause a variation in the output pulse; thus it is often necessary to stabilize the high-voltage supply.

A wide variety of photomultiplier tubes is available; choices may be determined by such parameters as physical size, response of photocathode to different incident wavelengths, sensitivity of photocathode, gain, noise level, and timing characteristics.

7.4 SEMICONDUCTOR DETECTORS

As we discussed in the previous section, solid semiconducting materials (germanium and silicon) are alternatives to scintillators for radiation detectors. Both Ge and Si form solid crystals in which the valence-4 atoms form four covalent bonds with neighboring atoms. All valence electrons thus participate in covalent bonds, and the band structure shows a filled valence band and an empty conduction band. The difference between an insulator and a semiconductor is in

the size of the energy gap, which is perhaps 5 eV in an insulator and 1 eV in a semiconductor. At room temperature a small number of electrons (perhaps 1 in 10^9) is thermally excited across the gap and into the conduction band, leaving a valence-band vacancy known as a "hole." As an electron from a neighboring atom fills the hole (creating in the process a new hole) the hole appears to migrate through the crystal (but of course the positively charged atoms do not move).

To control the electrical conduction in semiconductors, small amounts of materials called *dopants* are added. In the process of doping, atoms with valence 3 or 5 are introduced into the lattice. In the case of valence-5 atoms (P, As, Sb),

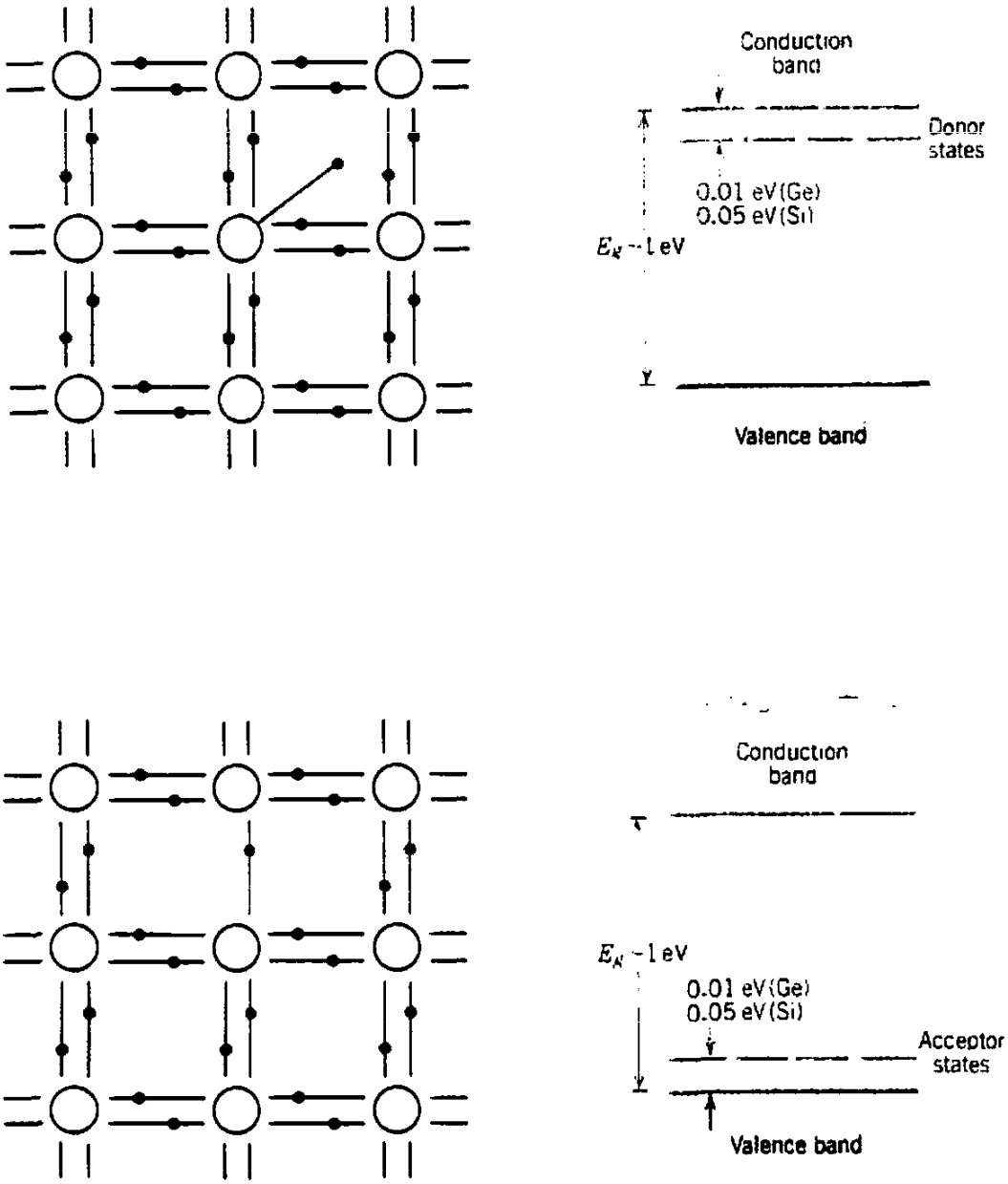

Figure 7.19 (Top) When a valence-5 atom replaces an atom of the crystal of Ge or Si, there is an extra electron that does not share in a covalent bond and that is easily excited into the conduction band. These atoms form donor states just below the conduction band. The material doped with the valence-5 impurity becomes an *n*-type semiconductor. (Bottom) When a valence-3 atom is used as the dopant, a vacancy or hole is formed which can easily accept an electron from the valence band. The hole can migrate through the material, which becomes *p*-type semiconductor.

four of the electrons form covalent bonds with neighboring Si or Ge; the fifth electron moves easily through the lattice and forms a set of discrete *donor states* just below the conduction band. Because there is an excess of negative charge carriers (electrons) this material is called *n-type semiconductor*. Alternatively, we could use valence-3 atoms, in which attempts to form covalent bonds with four neighboring atoms in the crystal would produce an excess of holes. These form *acceptor states* just above the valence band, and the material is called *p-type semiconductor* because the primary charge carriers are the positively charged holes. Figure 7.19 shows the band structure of the types of semiconductors.

It is useful to remember that *n*-type and *p*-type refer to the sign of the charge of the primary carriers of electric current. The materials themselves are electrically neutral.

When *p*-type and *n*-type materials are brought into contact, the electrons from the *n*-type material can diffuse across the junction into the *p*-type material and

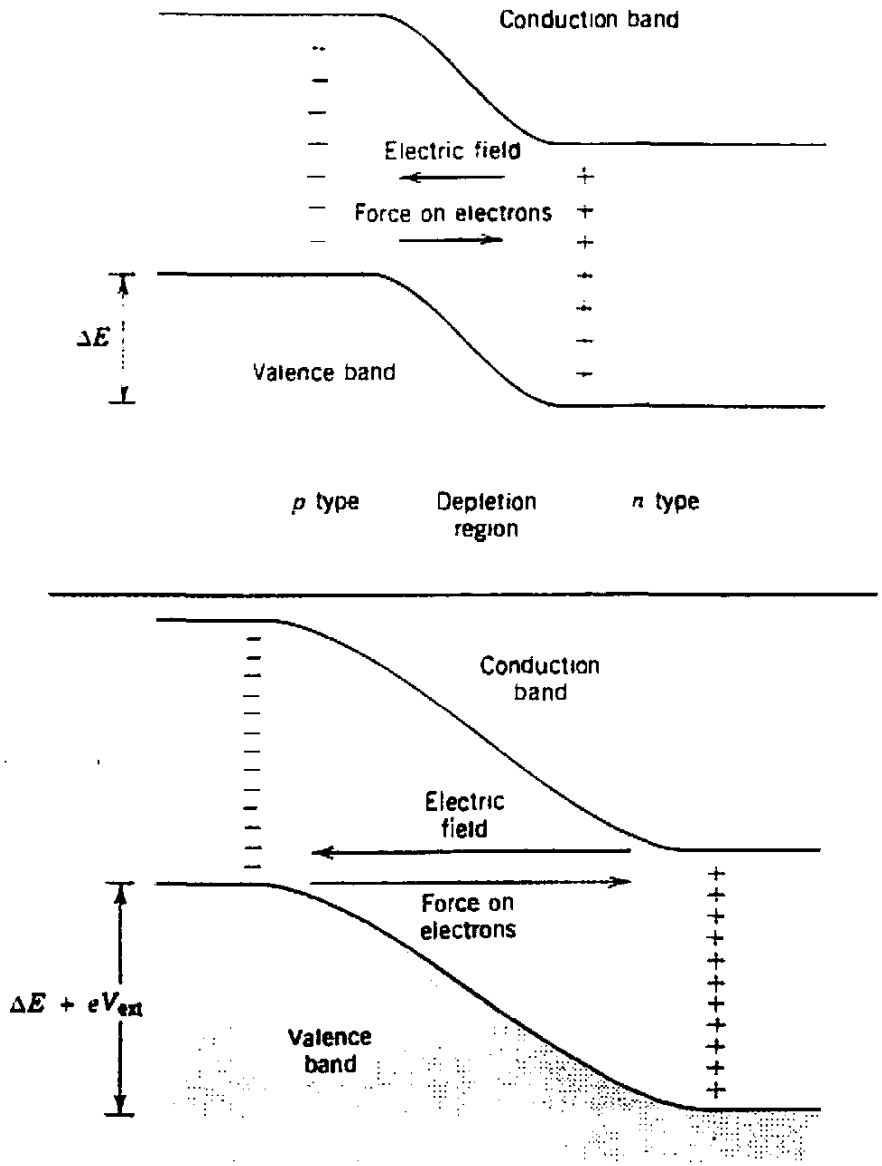

Figure 7.20 (Top) When *n*-type and *p*-type materials are brought into contact, electrons and holes near the junction can recombine to create a region that is depleted of charge carriers. (Bottom) Under reverse bias (when the − terminal of an external battery is connected to the *p*-type side), the depleted region becomes larger and the magnitude of the electric field increases.

combine with the holes; in the vicinity of the junction, the charge carriers are neutralized, creating a region called the *depletion region*. The diffusion of electrons from the *n*-type region leaves behind ionized fixed donor sites, while the similar diffusion of holes from the *p*-type region leaves behind negatively charged fixed acceptor sites. The space charge from the fixed sites creates an electric field which eventually halts further migration. The result, shown in Figure 7.20, is a *junction diode*.

If radiation enters the depletion region and creates electron-hole pairs, the result is very similar to that of an ionization chamber (in fact, the depletion region looks very much like a parallel-plate capacitor). Electrons flow in one direction, holes in the other, and the total number of electrons collected can form an electronic pulse whose amplitude is proportional to the energy of the radiation.

In practice, these detectors are operated with large reverse bias voltages (1000–3000 V), which has two effects: it increases the magnitude of the electric field in the depletion region, making charge collection more efficient, and it increases the dimensions of the depletion region (thereby increasing the sensitive volume of the detector) by forcing more carriers to drift across from one type of material to the other.

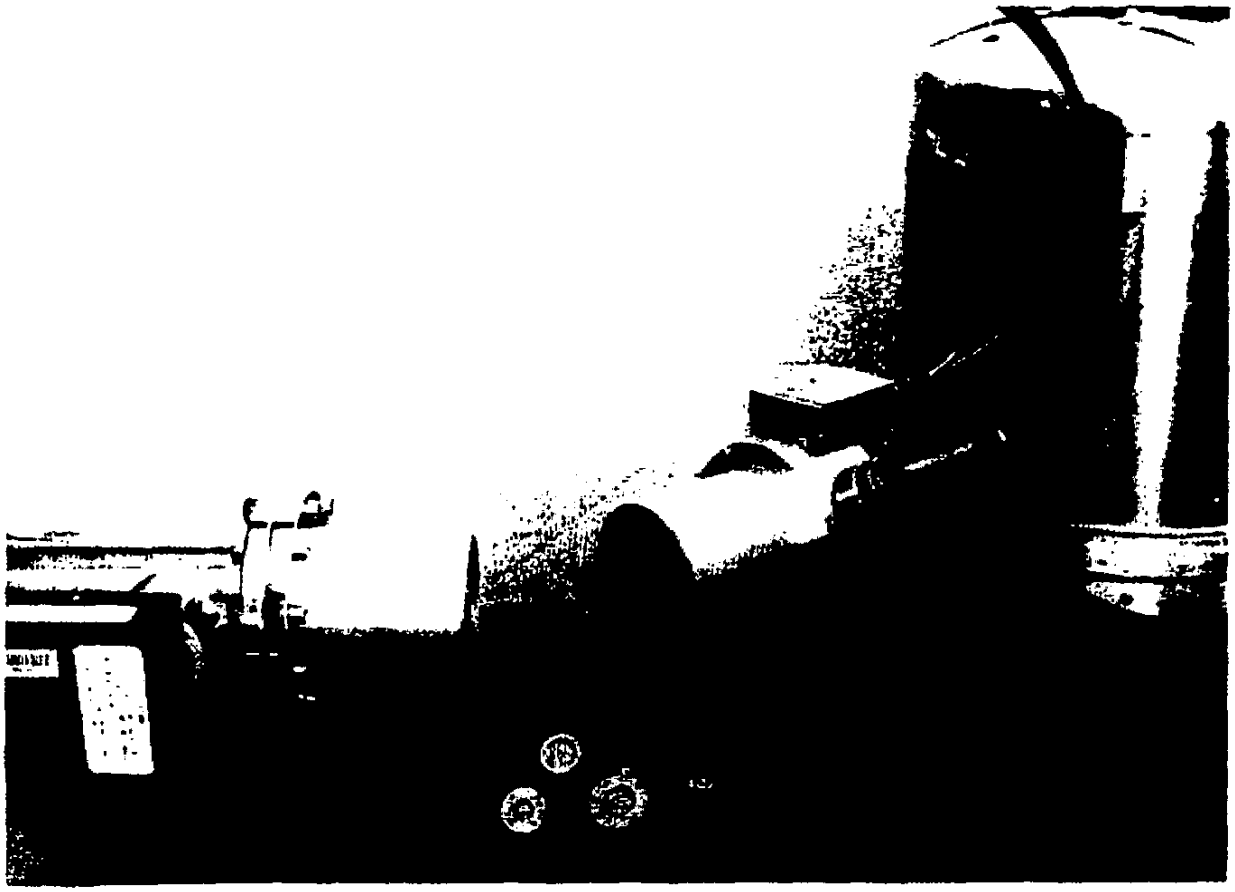

Figure 7.21 In the foreground are shown four different sizes of silicon surface-barrier detectors. Two large Ge γ-ray detectors are housed in the evacuated aluminum cryostats of diameter about 8 cm; the detectors are cylinders about 4 cm long and 4 cm in diameter. Each detector is mounted on a copper rod that is in thermal contact with a dewar of liquid nitrogen, one of which is visible at right. The small boxes mounted along the cryostats are preamplifiers.

One common fabrication procedure for Ge and Si detectors is to begin with a sample of *p*-type material and diffuse into its surface a concentration of Li atoms, which tend to form donor states and thereby create a thin *n*-type region. Under reverse bias, and at a slightly elevated temperature, the Li drifts into the *p*-type region, making quite a large depletion region. Such detectors are known as *lithium-drifted* Ge and Si detectors, or Ge(Li) and Si(Li) detectors (pronounced "jelly" and "silly"). Following the Li drift, the Ge(Li) detector must be kept cold (usually at liquid nitrogen temperature of 77 K); otherwise the Li will migrate out of its lattice sites in the depletion region and destroy the effectiveness of the detector. Keeping the detector cold also reduces the thermal excitation of electrons across the energy gap, thereby reducing the background electrical noise produced by the detector. Recently, large-volume, high-purity Ge detectors have become available, owing to advances in the techniques of refining Ge crystals. These detectors do not need to be kept at 77 K, but are operated at that temperature to keep the noise level low. Figure 7.21 shows a selection of solid-state detectors.

The *n*-type layer created in producing Ge(Li) or Si(Li) detectors is of order 1 mm thick, which is easily penetrable by medium-energy γ rays (the range of a 100-keV photon in Ge is about 4 mm and in Si about 2 cm). However, for charged particles the range is much smaller (for a 1-MeV electron, the range is about 1 mm in Si and Ge; for a 5-MeV α particle, the range is only 0.02 mm in Si and Ge), and such a layer would prevent the particles from reaching the depletion region. For charged-particle work, the preferred choice is the *surface-barrier* detector, in which an extremely thin *p*-type layer is etched or deposited on the surface of *n*-type Si. A thin layer of gold is then evaporated onto the front surface to serve as one electrical contact. The total thickness that the particles must penetrate to reach the depletion region is thus made to be about 0.1 μm.

The time necessary to collect the charge from a large-volume detector may be in the range of 10–100 ns; variations occur depending on the geometry of the detector (planar or coaxial) and on the point of entry of the radiation relative to the electrodes.

7.5 COUNTING STATISTICS

All laboratory measurements contain sources of uncertainty or error. Some originate with the properties of the measuring instrument (such as trying to estimate fractions of a millimeter on a meter stick graduated in millimeters). Others, of which radioactive decay is one, originate with the inherent statistical variations of a process whose occurrence is essentially random. If we make a single measurement of a phenomenon governed by a random, statistical process, then the outcome of the measurement is useful to us only if we can provide the answers to two questions: (1) How well does the measurement predict the outcome of future measurements? (2) How close to the "true" value is the outcome of a single measurement likely to be? To answer these questions, we must know how the various possible outcomes are distributed statistically.

Let us suppose we have a sample of N nuclei, and we wish to compute the probability $P(n)$ that n of them decay in a certain time interval. (For the moment we assume that we can measure time with arbitrarily small uncertainty.)

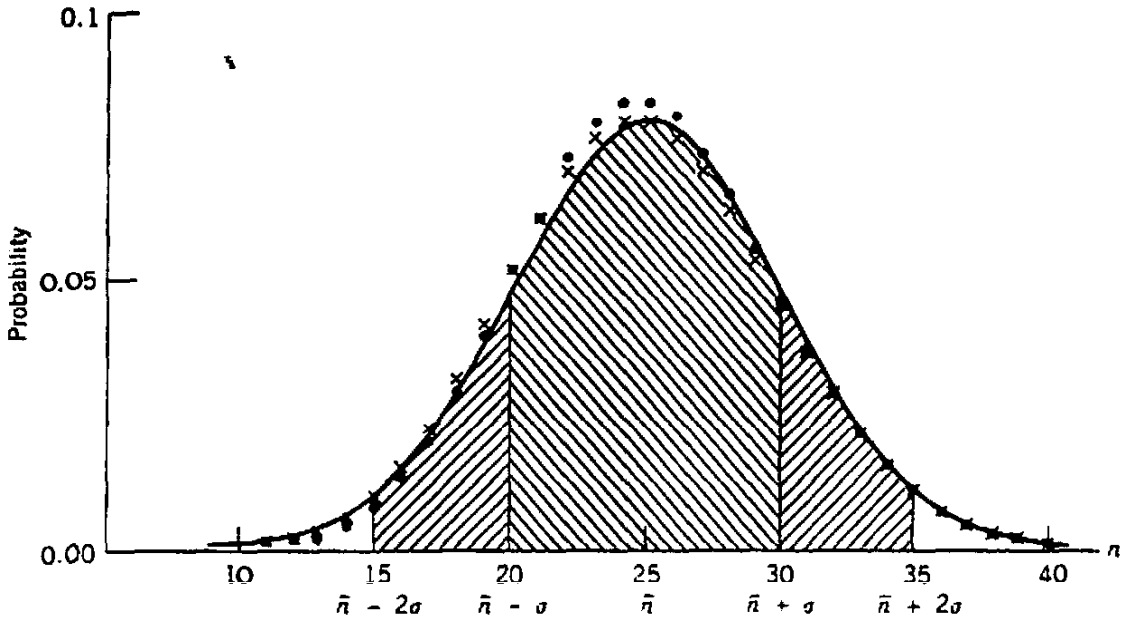

Figure 7.22 Comparison of binomial (●), Poisson (×), and Gaussian (—) distributions for $\bar{n} = 25$. The approximation of using the Gaussian distribution improves as $\bar{n}$ increases. The area under the Gaussian distribution between $\bar{n} - \sigma$ and $\bar{n} + \sigma$ is 68% of the total area under the curve; thus any single measurement has a 68% probability to be within $\pm\sigma$ of the true mean $\bar{n}$. The area between the limits $\bar{n} \pm 2\sigma$ is 95% of the total area.

The probability for decay of a single nucleus is p. We assume that p is constant —each nucleus decays independently of the state of the other nuclei. The desired probability can be found from the *binomial distribution*

$$P(n) = \frac{N!}{n!(N-n)!} p^n (1-p)^{N-n} \tag{7.24}$$

The binomial distribution is most often encountered in simple random experiments, such as tossing a coin or rolling dice. The distribution is shown in Figure 7.22 and is characterized by its mean $\bar{n}$, which is equal to pN (as one would guess —the decay probability per nucleus times the total number of nuclei gives the number of decays) and also by the *variance* σ^2:

$$\bar{n} \equiv \sum_{n=0}^{N} nP(n) = pN \tag{7.25}$$

$$\sigma^2 \equiv \sum_{n=0}^{N} (n-\bar{n})^2 P(n) = \bar{n}(1-p) \tag{7.26}$$

The *standard deviation* σ is a rough measure of the "width" of the statistical distribution.

When n and N are small, the binomial distribution is quite trivial to use, but when n and N are very large, as might be typical in decay processes, the distribution becomes less useful as the computations become difficult. We can obtain a less cumbersome approximation in the case when $p \ll 1$ (which will usually be true for radioactive decays):

$$P(n) = \frac{\bar{n}^n e^{-\bar{n}}}{n!} \tag{7.27}$$

where $\bar{n} = pN$ as before. This is known as the *Poisson distribution*. Note that the probability to observe n decays depends only on the mean value $\bar{n}$. For this distribution, $\sigma = \sqrt{\bar{n}}$.

Another useful approximation occurs in the case of small p and large $\bar{n}$ ($\gg 1$), in which case the *normal* or *Gaussian distribution* can be used:

$$P(n) = \frac{1}{\sqrt{2\pi\bar{n}}} e^{-(n-\bar{n})^2/2\bar{n}} \tag{7.28}$$

and once again, $\sigma = \sqrt{\bar{n}}$.

For most practical purposes, we can use the Gaussian distribution for our statistical analysis. As shown in Figure 7.22, the Gaussian distribution has the property that 68% of the probability lies within $\pm\sigma$ of the mean value $\bar{n}$. Unfortunately the mean value $\bar{n}$ is not available for measurement: it results only from an *infinite* number of trials. Clearly the "true" value we are seeking is represented by $\bar{n}$, and our single measurement n has a 68% chance of falling within $\pm\sigma$ of $\bar{n}$. We therefore take n as the best guess for $\bar{n}$ and we quote the error limit of n as $\pm\sigma$, or $\pm\sqrt{\bar{n}}$.

If we were to repeat the measurement a large number of times, we could trace out a histogram that should come fairly close to the Gaussian distribution, and the fractional error would be reduced each time. Suppose we made m independent measurements and recorded a total of M counts ($M = \sum_{i=1}^{m} n_i$). Then

$$\begin{aligned} \sigma_M &= \sqrt{\sum_{i=1}^{m} \sigma_i^2} \\ &= \sqrt{\sum n_i} \\ &= \sqrt{M} \end{aligned} \tag{7.29}$$

$$\bar{n} = \frac{M}{m}$$

$$\sigma_{\bar{n}} = \frac{\sigma_M}{m} = \frac{\sqrt{M}}{m} = \sqrt{\frac{\bar{n}}{m}} \tag{7.30}$$

The standard deviation (error) of our best estimate for the true value $\bar{n}$ has been reduced by the factor $1/\sqrt{m}$. Each successive independent measurement reduces the uncertainty of the mean.

Any quantity that has a random statistical distribution of this type (the probability for any one event is small and independent of other events; the number of observed events is large) has the fundamental property that the expected uncertainty in the number of observations can be estimated as the square root of the number of observations. This applies not only to counts observed in a detector of radioactive decays, but also to the production of ionizing events in the detector itself. As we see in the next section, the energy resolution of a detector is determined by the square root of the number of ionizing events.

Finally, a word of caution—the square-root relationship applies only to raw numbers of events, not to calculated quantities such as rates or differences

between numbers of counts. That is, if a detector records N counts in time t, the counting rate is N/t with an uncertainty of $N^{1/2}/t$. If we wish to subtract B background counts, the uncertainty in the difference $N - B$ is $(N + B)^{1/2}$, following the usual rules for propagation of error.

7.6 ENERGY MEASUREMENTS

A schematic diagram of the equipment that might be used to measure the energy of nuclear radiations is shown in Figure 7.23. The electronic signal from the detector usually goes directly to a *preamplifier* (preamp), which converts the charge pulse from the detector to a voltage pulse (for example, by charging a capacitor) and then drives the pulse to the next element in the circuit. The *amplifier* provides the voltage gain to bring the millivolt preamp pulse to the range of a few volts where it can conveniently be processed. The amplifier must be *linear*, so that the proportionality of radiation energy and pulse height can be preserved. The many pulse heights that may be produced by a complex decay process can conveniently be displayed on a *multichannel analyzer* (MCA) in histogram style, that is, with pulse height on the horizontal scale and number of pulses on the vertical. The input pulses are digitized, and the digital pulse height is stored in a memory location referred to as a *channel*; hence, the horizontal axis is often labeled as *channel number*. The resulting pulse-height *spectrum* can then be used to determine the energies of the radiations emitted by the source (from their locations on the horizontal scale) and their relative intensities (from the areas of the various peaks in the spectrum). This is most frequently done for γ radiation, which is now discussed in more detail.

Figure 7.24 shows some of the processes that can occur when a γ-ray photon enters a solid detector. The photon can Compton scatter several times; after each scattering, the photon loses some energy and a free electron is produced. Gradually the photon suffers either of two fates: it continues the repeated Compton scattering, eventually becoming so low in energy that photoelectric absorption occurs and the photon vanishes, or else it wanders too close to the edge of the crystal and scatters out of the crystal. The energy of the photon is converted into electrons (photoelectrons or Compton-scattered electrons), which have a very short range in the crystal, and which therefore lose energy very rapidly, by creating light photons in a scintillator or electron-hole pairs in a

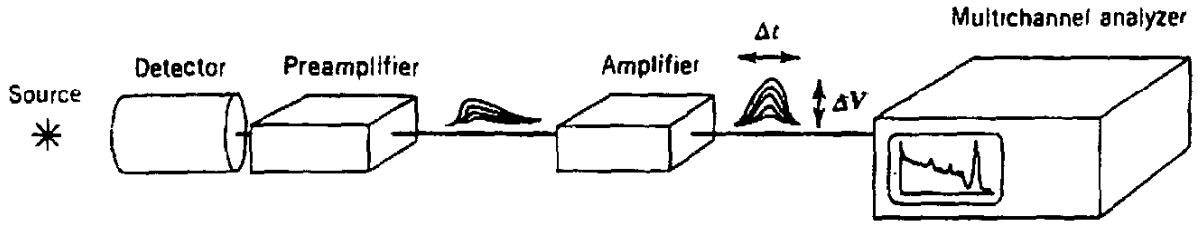

Figure 7.23 Schematic diagram of electronic equipment that might be used in a measurement of the energies of radiations emitted by a source. The pulses between the preamplifier and amplifier generally have a short (ns) rise time and a long (ms) decay time, with an amplitude of millivolts. The amplifier pulses are more symmetric, with a width Δt of μs and a pulse height ΔV of a few volts. The multichannel analyzer display shows ΔV on the horizontal axis.

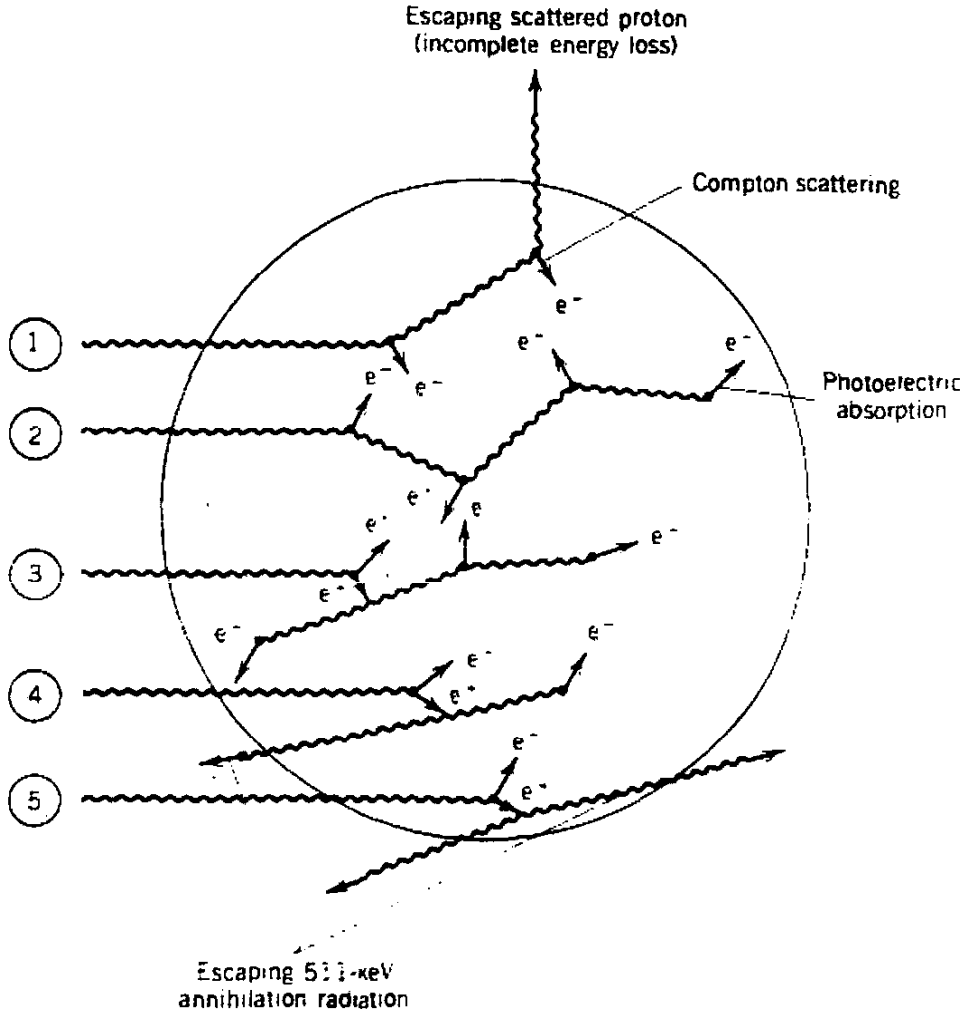

Figure 7.24 Processes occurring in γ-ray detection. (1) The photon Compton scatters a few times and eventually leaves the detector before depositing all its energy. (2) Multiple Compton scattering is followed by photoelectric absorption, and complete energy deposition occurs. (3) Pair production followed by positron annihilation, Compton scattering, and photoelectric absorption; again, complete energy loss occurs. (4) One of the annihilation photons leaves the detector, and the γ ray deposits its full energy less 511 keV. (5) Both annihilation photons leave the detector, resulting in energy deposition of the full energy less 1022 keV. Processes (4) and (5) occur only if the γ-ray energy exceeds 1022 keV.

semiconductor detector. We can assume that all of this energy is absorbed, and we will refer to this quantity as the energy deposited in the detector by the original photon. If the original photon eventually suffers photoelectric absorption, the energy deposited is equal to the original γ-ray energy. If it scatters out of the crystal, the energy deposited is less than the original photon energy.

Let's consider how much energy is given to the scattered electron in a single Compton event. From Equation 7.15, we can find the electron kinetic energy:

$$T_e = E_\gamma - E'_\gamma = \frac{E_\gamma^2(1 - \cos\theta)}{mc^2 + E_\gamma(1 - \cos\theta)} \tag{7.31}$$

Since all scattering angles can occur in the detector, the scattered electron ranges in energy from 0 for $\theta = 0°$ to $2E_\gamma^2/(mc^2 + 2E_\gamma)$ for $\theta = 180°$. These electrons will normally be totally absorbed in the detector, and (if the scattered photons escape) they contribute to the energy response of the detector a continuum called

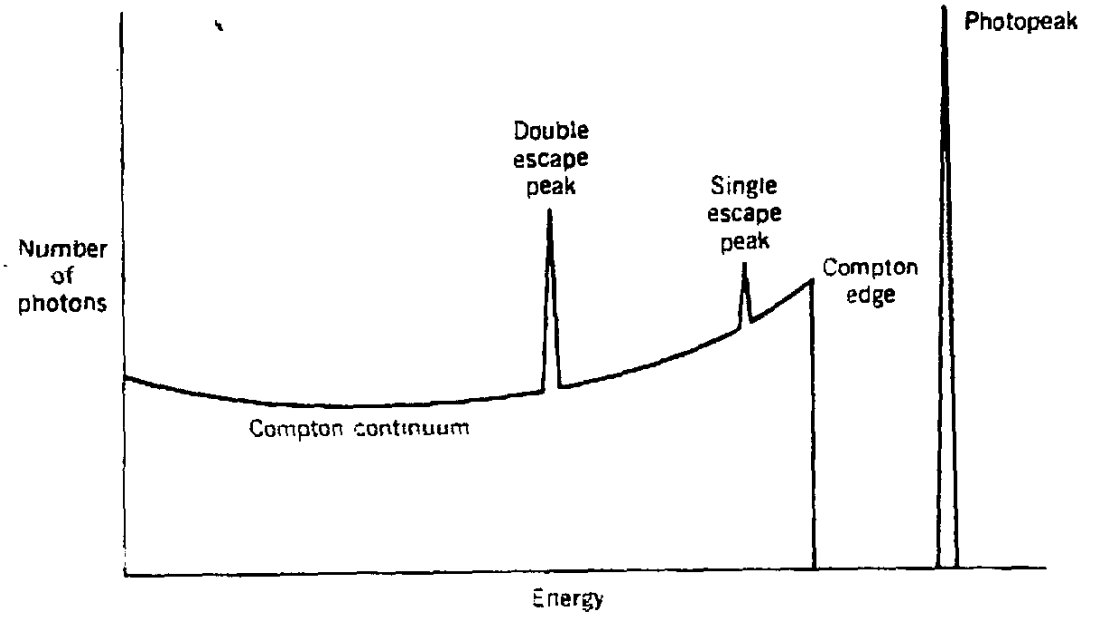

Figure 7.25 A typical response of a detector to monoenergetic γ rays. The photopeak results from the γ ray losing all its energy in the detector, as in events 2 and 3 in Figure 7.24. The Compton continuum consists of many events of type 1, while the single- and double-escape peaks result from processes 4 and 5. The detector energy resolution might tend to broaden all peaks more than they are shown here, and multiple Compton scattering will fill in the gap between the Compton edge and the photopeak. The escape peaks appear only if the γ-ray energy is above 1.022 MeV.

the *Compton continuum*, ranging from zero up to a maximum known as the *Compton edge*. (This continuum is not flat: the Klein-Nishina formula, Equation 7.16, shows how the Compton scattering probability varies with angle.) The peak at $E = E_\gamma$ corresponding to complete photoelectric absorption (called the *full-energy peak* or *photopeak*) and the Compton continuum are shown in Figure 7.25.

We have so far neglected the third process of γ-ray interactions in the detector, that of pair production. The positron and electron are created with a total kinetic energy of $E_\gamma - 2mc^2$, as in Equation 7.18, and loss of that energy in the detector would result in a peak at the full energy. However, once the positron slows down to an energy near that of the atomic electron, *annihilation* takes place, in which the positron and an atomic electron disappear and are replaced by two photons of energy mc^2 or 511 keV. These two photons can travel out of the detector with no interactions, or can be totally or partially absorbed, through Compton scattering processes. We therefore expect to see peaks at $E_\gamma - 2mc^2$ (when both photons escape), $E_\gamma - mc^2$ (when one escapes and the other is totally absorbed), and E_γ (when both are totally absorbed). These single- and double-escape peaks are shown in Figure 7.25.

The relative amplitudes of the photopeak, Compton continuum, and escape peaks depend on the size and shape of the detector. In general, the larger the detector, the smaller is the Compton continuum relative to the photopeak, for there is a smaller chance of a Compton-scattered photon surviving from the center to the surface without interacting again. Similarly, in a large detector, there is a greater chance of capturing one or both of the 511-keV annihilation photons.

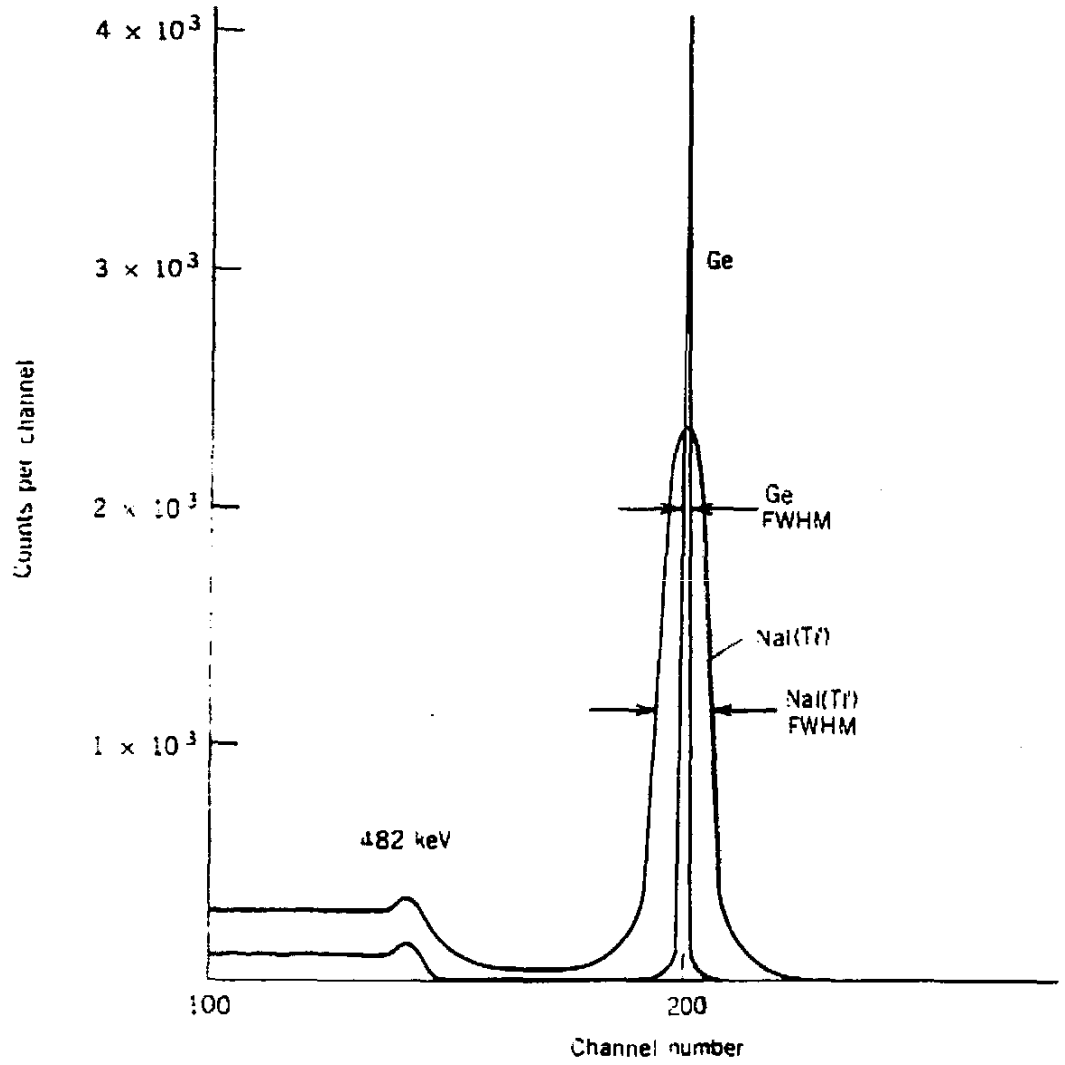

Figure 7.26 Comparison of NaI(Tl) and Ge(Li) spectra of ^{137}Cs. The energy of the photopeak is 662 keV. The resolution (FWHM) of the NaI(Tl) is about 40 keV, while that of the Ge is about 1 keV. The intensity (peak area) of the Ge is about 11% that of NaI(Tl).

Figure 7.26 shows MCA spectra of the decay of ^{137}Cs, such as might be obtained with Ge and NaI(Tl) detectors. Only a single γ ray, of energy 662 keV, is emitted in this decay. The Compton continuum is easily seen, as is the Compton edge. The "valley" between the Compton edge and the photopeak does not go quite to zero and the Compton edge itself is not sharp; in our previous discussion we assumed the Compton continuum to originate from a single-scattering event, and multiple-scattering events will distort the simple picture of Figure 7.25. The Compton edge is expected at $E = 478$ keV, in agreement with the observed spectrum.

What is striking about the two spectra shown are the differences in efficiency (essentially, the area of photopeak) and in resolution (the width of the photopeak) between Ge and NaI(Tl). NaI detectors have higher efficiencies than Ge detectors, and in addition have the advantages of lower cost (1/10 or less of the Ge cost) and simpler operating conditions (no cooling is required for NaI). Because the present demands of nuclear spectroscopy require the study of ever more complex decays, resolution has become of critical importance; to study these decays carefully, one must be able to determine all γ-ray energies and

intensities, which would not be possible if all peaks had widths characteristic of NaI(Tl) detectors. Early work with Ge detectors suffered a considerable loss in efficiency to obtain the good resolution; these detectors had efficiencies only a few percent of NaI(Tl) detectors. Improvements in refining techniques of Ge have enabled the production of large-volume Ge detectors that are now only a factor of 2–3 below NaI(Tl) in efficiency. Because Ge has a lower atomic number than NaI, it will always have smaller interaction probabilities for photons and therefore smaller relative efficiency, the photoelectric absorption coefficient varying roughly as Z^4.

Let's now try to understand the reasons for the observed resolutions based on the statistics of the detection process.

The full-energy peaks of both NaI(Tl) and Ge detectors can be approximated as Gaussian shapes, and the width is characterized by the parameter σ in the general form of the Gaussian distribution

$$f(E) = A e^{-(E-\bar{E})^2/2\sigma^2} \tag{7.32}$$

where A is a normalization constant. The relationship between the mean $\bar{E}$ and σ cannot be used because we do not know the number of events $\bar{n}$ that are represented in the mean. (Recall that $\sigma = \sqrt{\bar{n}}$ holds only for counting events.)

Generally the width is specified in terms of the full width at half maximum (FWHM), that is, the distance ΔE between the two points E_1 and E_2 where $f(E_1) = f(E_2) = A/2$. A bit of manipulation gives

$$\Delta E = 2\sigma\sqrt{2\ln 2} \cong 2.35\sigma \tag{7.33}$$

Often the FWHM is expressed as a ratio $\Delta E/\bar{E}$.

To estimate σ, we must estimate $\bar{n}$, the number of statistical events associated with the production of the detector signal. The incident γ-ray energy is 662 keV. In NaI(Tl) the scintillation efficiency (the fraction of the incident radiation converted into light) is about 13%; thus 86 keV of photons appear. The energy per photon in NaI is about 4 eV, and the number of light photons is thus (on the average) about 21,000. The contribution to the resolution from this is about $2.35\sqrt{21{,}000}/21{,}000$ or about 1.6%. At the photocathode, the number is reduced even further. The transmission of the light through the glass end of the photomultiplier tube is typically about 85%, and the *quantum efficiency* of a typical photocathode (that is, the number of photoelectrons emitted per incident photon) is typically 23%. Thus the number of photoelectrons is only about 20% of the number of incident photons, or about 4200, and the contribution to the resolution is about $2.35\sqrt{4200}/4200$, or 3.6%. The electron multiplication process in the photomultiplier will increase the number of events and give a smaller contribution to the FWHM. *In the entire NaI(Tl) detection process, the smallest number of events corresponds to the production of electrons at the photocathode, and this is therefore the most substantial contributor to the energy resolution.*

This simple calculation has ignored a number of effects in the crystal, photomultiplier, and amplifier, all of which can make nonstatistical contributions to the resolution. A figure of 6% (40 keV) might be more typical at 662 keV. The absolute FWHM (the width of the energy peak) increases with energy, roughly as $E^{1/2}$, but the ratio $\Delta E/E$ decreases like $E^{-1/2}$; thus at 1 MeV, the resolution should be about 5% (50 keV).

In a Ge detector, there is only a single event contributing to the statistics—the creation by the photon of electron-hole pairs. In Ge, it takes on the average about 3 eV to create an electron-hole pair, and thus the mean number of statistical events when a 662-keV photon is fully absorbed would be about 220,000. The contribution to the resolution is then about 3.3 keV (by convention, NaI resolutions are usually expressed as percentages, and Ge resolutions in keV). This gives a resolution more than an order of magnitude better than NaI(Tl), and this difference can be understood simply on the basis of the properties of the absorption of radiation in the detectors.

We have failed to include a number of factors in our estimate for the Ge resolution. The absorption is in fact not well described by Poisson statistics; proper consideration of the statistical nature of the process (done empirically) reduces the calculated value to about 1.0 keV. Nonstatistical processes (collection of charges by the electric field, electronic noise in the preamp and amplifier) will tend to increase the value somewhat. A typical value for a good detector today is 1.7 keV at 1332 keV (the energy of a ^{60}Co γ-ray, taken as the standard for resolution measurement), which would correspond to about 1.2 keV at 662 keV, if the $E^{1/2}$ dependence is valid.

In γ-ray (or other radiation) spectroscopy measurements, the goal is usually to determine the energy and the intensity of the radiation. To find the energy, the centroid of a peak must be determined. For isolated, well-resolved peaks, the centroid can be determined by a simple numerical procedure. First it is necessary to subtract the background. (The peak may be on the Compton continuum of other peaks higher in energy.) This is usually done by drawing a straight line between groups of background channels above and below the peak (Figure 7.27). In this case a linear background is assumed, and the background counts can be

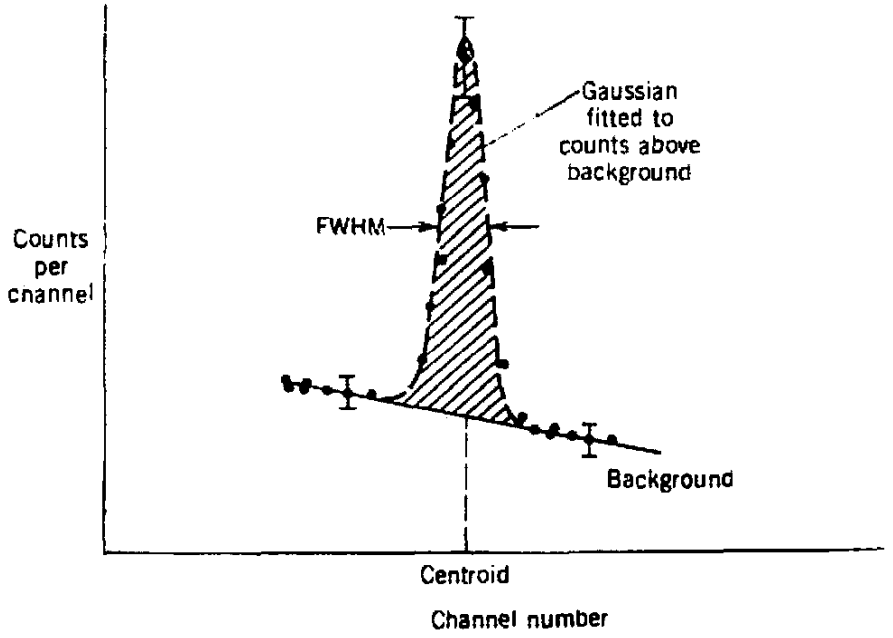

Figure 7.27 The area of a well-resolved peak can be found by subtracting a linear background and then either adding the counts above background or fitting a Gaussian function to the counts above background. Because the number of counts in each channel results from a simple counting process, its uncertainty is just the square root of the number; this applies only to the total number in each channel and *not* to the number above background.

subtracted directly. The centroid and area can then be determined by

$$\text{area} = \sum y_i \tag{7.34}$$

$$\text{centroid} = \frac{\sum x_i y_i}{\sum y_i} \tag{7.35}$$

where y_i represents the net number of counts above background in channel i. A slightly more sophisticated method is to fit a Gaussian function to the peak. This can be done most easily by assuming the functional dependence of the form of Equation 7.32 and taking the logarithm:

$$\ln y_i = \ln A - \frac{(x_i - \bar{x})^2}{2\sigma^2} \tag{7.36}$$

A least-squares fit to this form gives the parameters $\bar{x}$, σ, and A. Integrating the Gaussian form gives

$$\text{area} = \sigma A \sqrt{2\pi} \tag{7.37}$$

In the case of complicated spectra, this simple procedure will not work. Often backgrounds are not at all well represented by the linear approximation. Close-lying peaks that may overlap cannot be fitted in this way. Even the assumption of a Gaussian shape is not always valid, as there may be exponential "tails" on the high-energy or low-energy sides of the Gaussian. In this case, there are sophisticated fitting programs that can handle many parameters, including centroids and areas of many peaks and backgrounds of nonlinear shape.

Once we have values for the centroid and area of a peak, we would like to use those values to obtain the energy and counting rate for the radiation. To find the energy, it is necessary to calibrate the MCA so that channel number can be converted to energy. This is usually done with two or more radiations of known energy E_1 and E_2, which would be found to have centroids $\bar{x}_1$ and $\bar{x}_2$. It is then

Table 7.2 Commonly Used Energy Calibration Standards

Nuclide	$t_{1/2}$	Radiation	Energy (keV)
^{109}Cd	453 d	γ	88.037 ± 0.005
^{57}Co	271 d	γ	122.06135 ± 0.00013
			136.47434 ± 0.00030
^{198}Au	2.696 d	γ	411.80441 ± 0.00015
^{137}Cs	30.17 y	γ	661.661 ± 0.003
^{60}Co	5.271 y	γ	1173.238 ± 0.015
			1332.513 ± 0.018
^{207}Bi	38 y	e^-	481.65 ± 0.01
			975.63 ± 0.01
^{241}Am	433 y	α	5485.74 ± 0.12
^{226}Ra	1600 y	α	4784.50 ± 0.25
			5489.66 ± 0.30
			6002.55 ± 0.09
			7687.09 ± 0.06

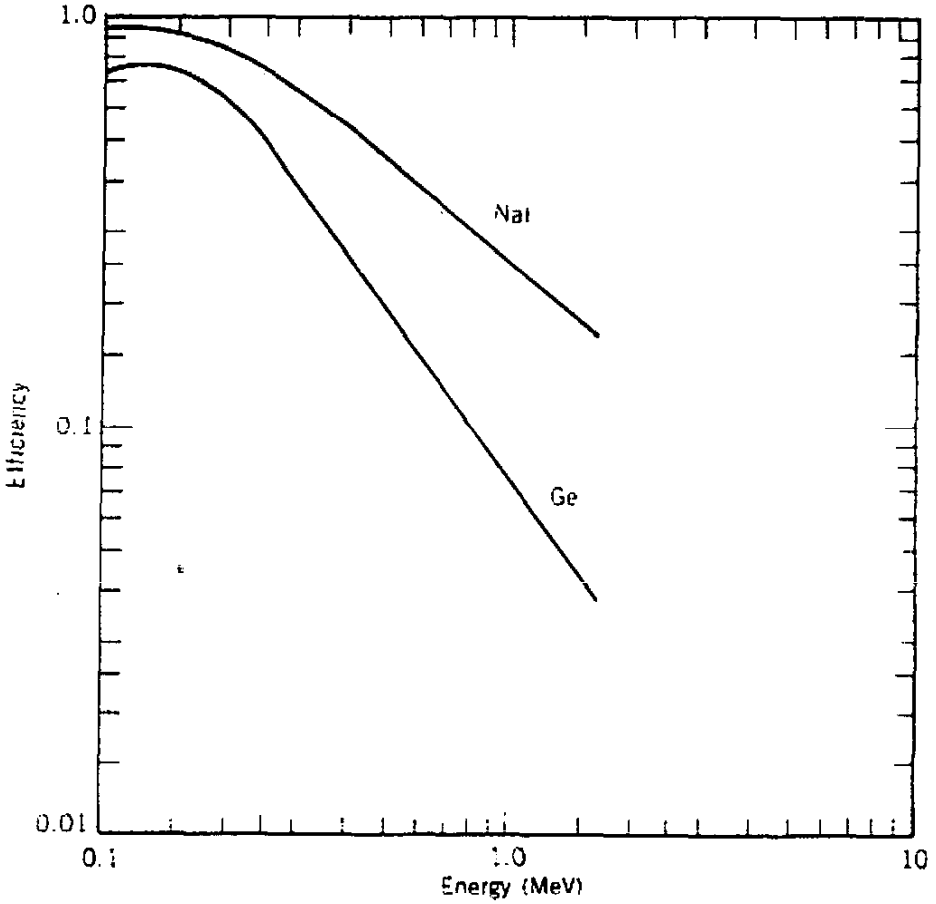

Figure 7.28 Relative efficiencies of NaI and Ge detectors. Here "efficiency" means the probability that a photon *striking the detector* will appear in the photopeak; it does not take into account the differing sizes of the detectors. The curves are drawn for a 3-in.- diameter by 3-in.-long NaI(Tl) and a 4.2-cm-diameter by 4.2-cm long Ge, with the source at 10 cm from the detector. In the terms that are usually used to specify relative efficiencies, the relative probability for a 1.332-MeV photon (emitted by ^{60}Co) to appear in the Ge photopeak is 8% that of the NaI(Tl) photopeak, including the solid angle factor.

easy to find a linear relationship between $\bar{x}$ and E. Because MCAs (and other parts of the system, including the detector and amplifier) may be slightly nonlinear, it is advisable to choose calibration energies E_1 and E_2 as close as possible to the unknown energy E. It is necessary to use two radiations for calibration because channel zero of the MCA will not necessarily correspond to a pulse height of zero. Table 7.2 shows some commonly used calibration standards.

To convert the peak area to an absolute counting rate, we must know something about the efficiency of the detector—how large a solid angle does it subtend at the source of the radiation and what is the probability that an incident radiation will be absorbed into the photopeak? The detector efficiency depends on the energy rather dramatically for γ rays; Figure 7.28 shows the absolute efficiency of NaI(Tl) and Ge detectors as a function of the γ-ray energy.

7.7 COINCIDENCE MEASUREMENTS AND TIME RESOLUTION

When we wish to study radiations that follow one another in cascade—for example, γ rays that follow a particular β decay—equipment of the type shown in Figure 7.29 is often used. One primary object of this equipment is to determine

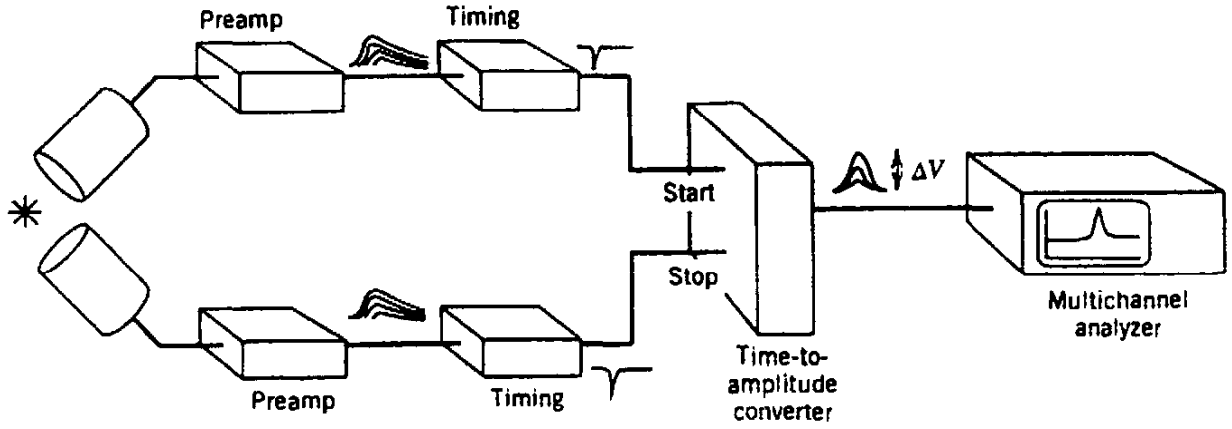

Figure 7.29 Schematic diagram of equipment to determine whether two radiations from the source are in time coincidence (that is, whether they come close enough together in time to originate from the same nucleus in a sequential or cascade emission). The short rise time of each preamp signal triggers a timing circuit; the fast timing signals start and stop a time-to-amplitude converter (TAC), the output of which has a pulse height ΔV that is proportional to the time difference between the start and stop pulses. The spectrum of pulse heights (and therefore of times) can be displayed on a MCA.

whether the second radiation is in true time coincidence with the first. That is, do the two radiations come close enough together in time to originate from the same nucleus in a sequential or cascade emission? The time-to-amplitude converter (TAC) produces a time spectrum of output pulses whose pulse height is proportional to the difference in arrival times of the two input pulses; this in turn, after correcting for known delays in the intervening equipment and signal cables, must be related to the difference in emission times of the two radiations from the source.

A time coincidence of two radiations from the same nucleus is called a *true* or *real* coincidence. It is also possible for radiations from different nuclei to trigger the timing circuits; this produces an unwanted *chance* or *accidental* coincidence. In principle, discriminating between true and chance coincidences is relatively easy. After accepting the first radiation in the start channel of the TAC, we wait only a very short time (perhaps nanoseconds) for the second radiation to arrive and trigger the stop channel. The longer we must wait, the greater is the possibility for a radiation from a different nucleus to produce a chance coincidence. (We are assuming in this discussion that the time interval between the emission of the two radiations in the nucleus is negligibly short. The case in which this is not true is treated in the next section.) The pulse height spectrum provides a relatively trivial means to distinguish between true and chance coincidences. The pulse heights, and thus the time differences, corresponding to start and stop signals from true coincidences have a definite fixed time relationship. Chance coincidences, representing emissions from different nuclei, have no definite time relationship; if the decay rate from the source does not change, it will be just as probable to find the second radiation emitted (from a different nucleus) at any time following the first radiation. Chance coincidences produce a uniform range of pulse heights whereas true coincidences produce a single unique pulse height. Figure 7.30 illustrates the MCA display of the TAC spectrum that might result.

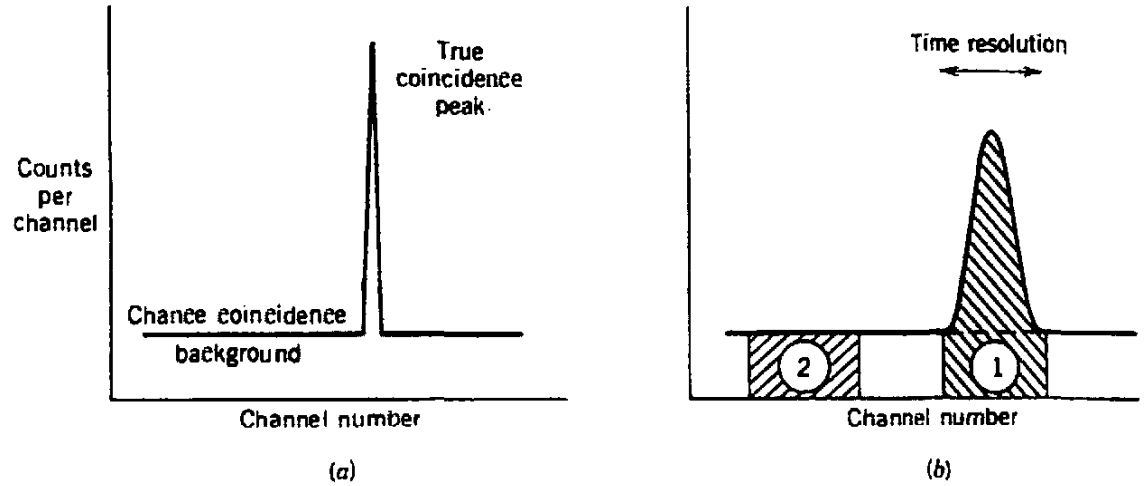

Figure 7.30 Time-to-amplitude converter spectrum of coincidences for (*a*) ideal detectors and (*b*) real detectors. The pulse height (running along the horizontal axis, as in all MCA spectra) gives the time difference between the two pulses. The time jitter in real detectors broadens the true-coincidence peak. The area in pulse-height region 1 gives true + chance coincidences; if the background is flat, region 2 gives the chance coincidences, and the difference gives the true coincidences only.

Figure 7.30*a* illustrates the situation for ideal detectors and electronics, in which the timing signal is derived from the radiation entering the detector with no ambiguities or uncertainties. Actual detectors and electronics can introduce distortions (from electronic noise, for example, or from difficulties in triggering the timing circuit from the preamp pulse), and the resulting time spectrum is shown in Figure 7.30*b*. The sharp peak of true coincidences is broadened; it has a width that is characteristic of the *time resolution* τ of the detector and electronics system. To determine the rate of true coincidence emissions, we could electronically select regions 1 and 2 in Figure 7.30*b*, and the difference in their areas (if we are confident that the chance coincidence background is flat) gives the true coincidence peak.

By using this procedure, we can always correct for the chance coincidences. But if the chance rate is too high, the statistical uncertainties introduced by subtracting two large and nearly equal quantities can result in a deduced true coincidence rate with a relatively large uncertainty. It is therefore usually advisable to try to reduce the chance coincidence rate to the smallest possible level. This can be done in two ways. (1) Because the chance coincidence rate depends on the random overlap in time of two pulses, it increases as the square of the activity of the source. Doubling the activity, for example, increases the true coincidence rate by a factor of two but the chance rate increases by a factor of four. Reducing the activity therefore reduces the rate of chance coincidences. Reducing it too much, on the other hand, can reduce the rate of true coincidences so much that the statistical precision is degraded; therefore, compromises are necessary in adjusting the activity of the source. (2) Optimizing the detector and electronics can reduce the time resolution of the true coincidence peak in Figure 7.30*b*, which means that the corresponding chance coincidence background that must be counted is similarly reduced. The time resolution ultimately depends on the influence of random noise in the detector and electronics or in the variations

in the time necessary to collect the electronic charges in the detector that form the preamp pulse. With Ge detectors, especially the large-volume crystals that are presently used for γ ray detection, the charge collection time over the volume of the detector can limit the resolution to about 10 ns. For small NaI detectors with fast photomultipliers, values in the range 1 ns are possible, and plastic scintillators permit even smaller values, down to perhaps 100 ps.

7.8 MEASUREMENT OF NUCLEAR LIFETIMES

Techniques for measuring nuclear lifetimes are as varied as the lifetimes themselves—from more than 10^{15} y for some naturally occurring radioisotopes to below 10^{-15} s for short-lived excited states. Searches for double-β decay (see Chapter 9) are conducted in the range of lifetimes of about 10^{20} y, and the breakup of highly unstable nuclei such as ^{8}Be and ^{5}He occurs with lifetimes in the range of 10^{-16} to 10^{-20} s. We will not discuss here the unusual techniques needed for these special cases, but instead we shall give examples of a few techniques for measuring lifetimes that are more commonly encountered in studying nuclear decays.

The most straightforward technique is of course to observe the exponential decay of activity as a function of time, such as was shown in Figure 6.1. Plotting $\mathscr{A}$ against t on a semilog scale gives the decay constant λ directly, and thus the half-life. For half-lives in the range of minutes to hours, this is a particularly easy laboratory exercise. We can count a certain type of radiation and display the accumulated counts on a scaler. This same technique can be used for half-lives in the range of years, although it is less convenient to follow the decay for several half-lives. As we get to significantly longer half-lives, this method becomes impractical. Figure 7.31 shows an example of this direct technique.

For very long half-lives, it is better to use the method of *specific activity*. (Specific activity indicates the quantity of activity per unit of substance, such as Ci per gram.) Here we can use the expression $\mathscr{A} = \lambda N$ directly. We can determine $\mathscr{A}$ by counting the number of decays emitted in a certain period of time, and we can determine N (the number of radioactive nuclei) by such techniques as chemical analysis or mass spectrometry.

When we go to half-lives shorter than minutes, we must deal with our inability as experimenters to perform the measurement of $\mathscr{A}$ vs t. That is, suppose we had a decay with a 10-s half-life. We would hardly have time to take one data point and clear the scaler for the next before the sample would have decayed away. For this range, we can take advantage of a capability built into most multichannel analyzers, called *multiscaling*. In this mode of operation, the MCA accepts a logic pulse rather than a linear pulse. A variable *dwell time* can be set by the experimenter. The MCA starts in channel 1 and counts the number of logic pulses that arrive during the dwell time. It stores that number in channel 1, then moves to channel 2 and repeats the cycle. The MCA thus does all the reading and recording of the scalers for us, and we should be able simply to watch the display screen as decay curves similar to Figure 6.1 appear.

In principle we could extend this technique to shorter and shorter half-lives, but we face a limitation at about 10^{-3} s. Most radiation detectors cannot

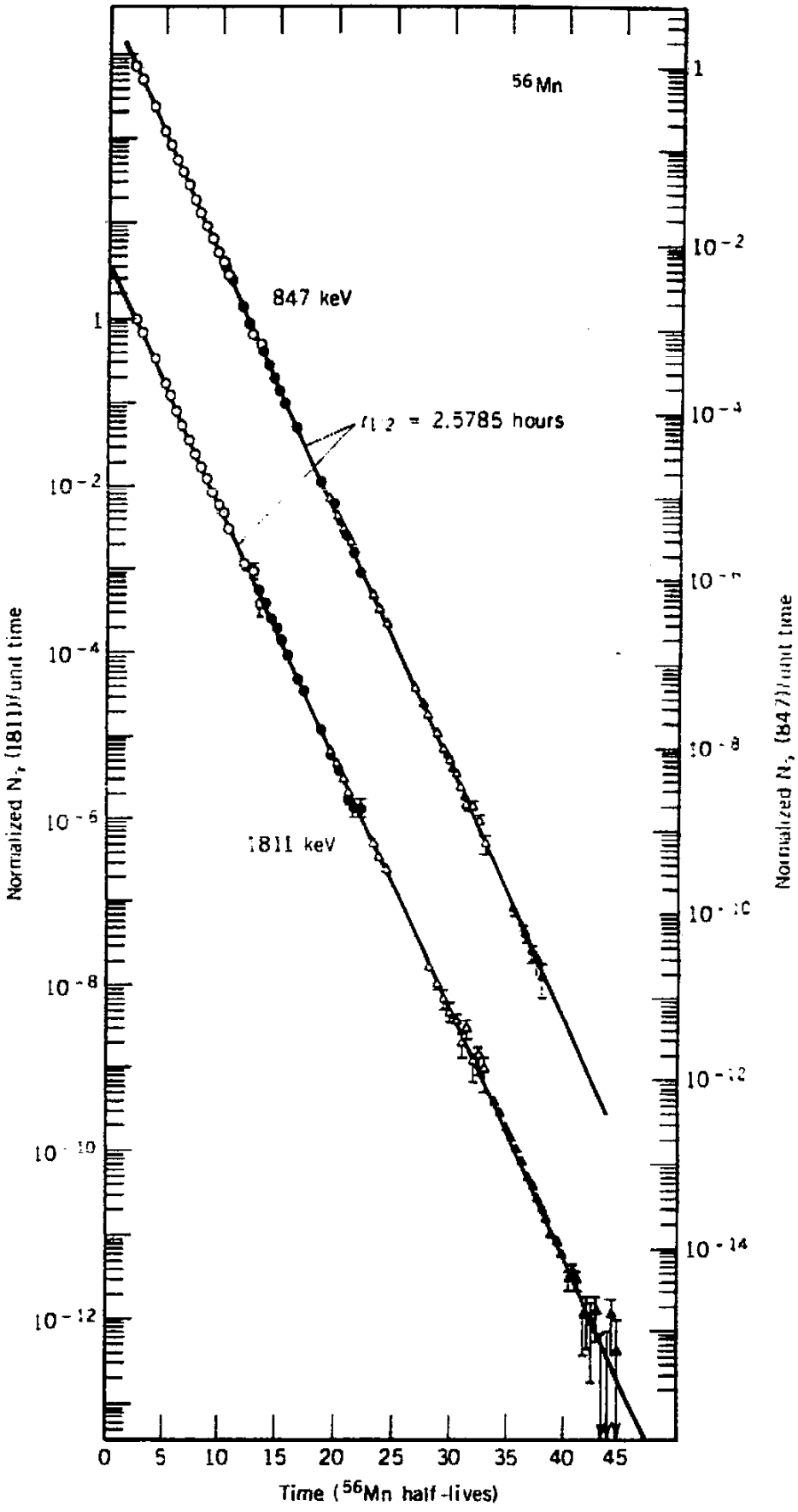

Figure 7.31 Direct measurement of half-life from the decay of activity with time. Data from two different γ rays in the decay of ^{56}Mn are plotted against time on a semi-log scale over 45 half-lives. During this period the count rate changes by more than 13 orders of magnitude. From E. B. Norman, S. B. Gazes, and S. G. Crane, *Bull. Am. Phys. Soc.* **30**, 1273 (1985); courtesy E. B. Norman.

accommodate counting rates in excess of 10^5/s. If we set the dwell time at 10^{-3} s, then we would accumulate a maximum of only about 100 counts per channel, and each channel would have an uncertainty of the order of $1/\sqrt{100}$, or 10%, resulting in a large uncertainty of the half-life.

We can measure half-lives shorter than 10^{-3} s if we have a precise way of determining the time interval between the formation of a nuclear state and its decay. The formation of a state is signaled by the observation of a radiation that leads to that state. We thus can do a *coincidence* experiment between a radiation that populates a state and a radiation from its decay. The easiest way to accomplish this is with the time-to-amplitude converter (TAC) as was shown in Figure 7.30 for cases in which the nuclear state has a half-life that is very short compared with the time resolution. If the half-life of the state is comparable to or greater than the time resolution, the TAC spectrum will show evidence of the usual sort of exponential decay that is shown by all radioactive systems. That is, the probability for the state to survive for a time t after its formation decreases exponentially as the time t increases. It is thus most probable that we will observe the second radiation within a short time after the formation of the state; the longer we wait, the less probable it is for the state to have survived and the

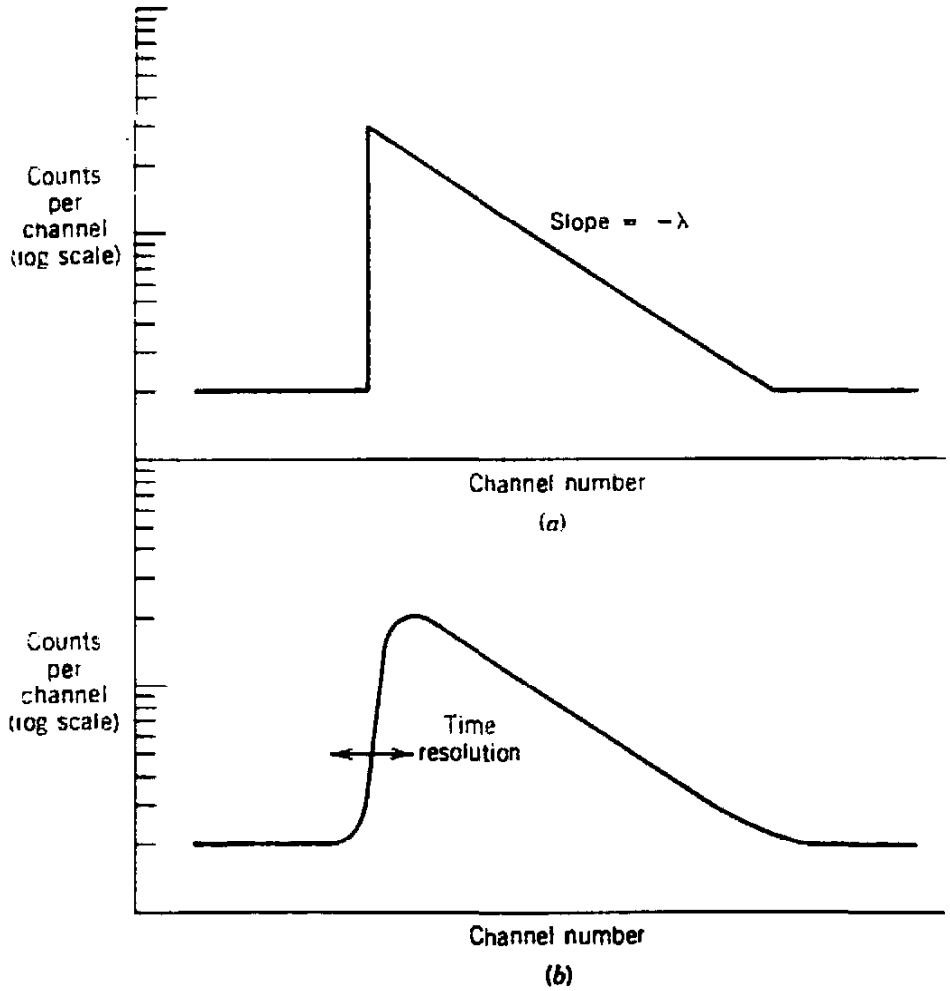

Figure 7.32 If the nuclear state between the first and second radiations has a half-life that is *not* negligibly short compared with the time resolution, we can observe its exponential decay. These TAC spectra should be compared with those of Figure 7.30 to see the effect of the decay of the state. (*a*) Ideal detectors, (*b*) real detectors.

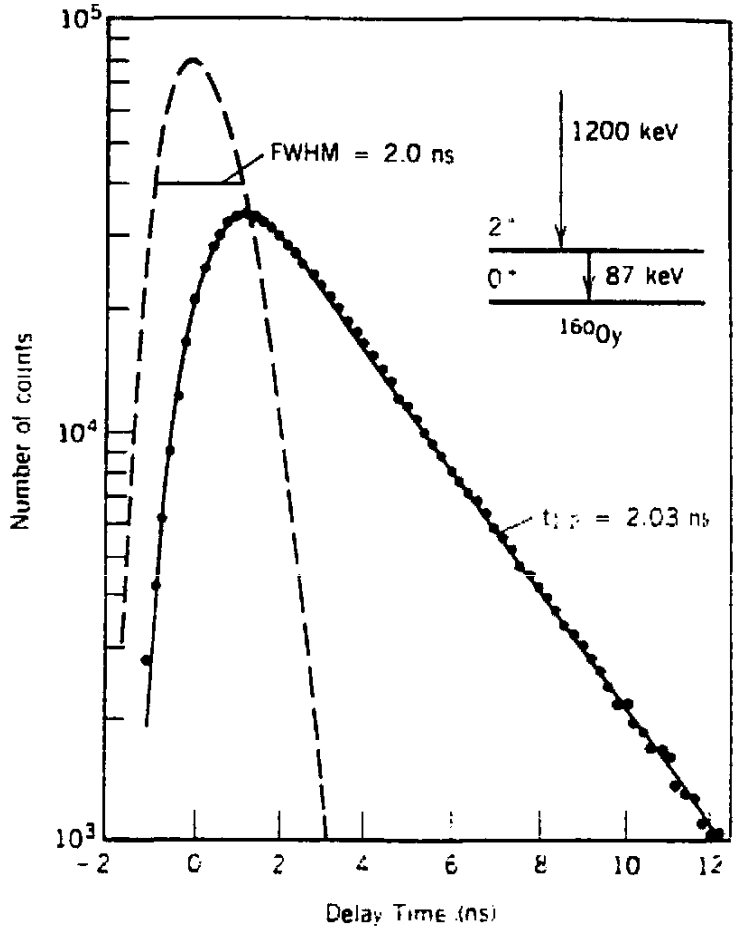

Figure 7.33 An example of a half-life measurement by the delayed coincidence technique. The dashed line shows the response expected for two radiations emitted essentially instantaneously, that is, within a time that is small compared with the time resolution of the system (2 ns); this is the so-called "prompt" curve. The delayed curve shows the rounding, as in Figure 7.32, owing to the finite time resolution. From the linear portion of the semilog plot, a half-life of 2.03 ± 0.02 ns is deduced for the 87-keV first excited state in ^{160}Dy. Data from P. C. Lopiparo, R. L. Rasera, and M. E. Caspari, *Nucl. Phys.* **A178**, 577 (1972).

fewer of the second radiations we count. The resulting TAC spectrum is shown in Figure 7.32.

This type of experiment is an example of the *delayed coincidence* technique. An example of experimental results using this technique is shown in Figure 7.33.

The limitation on the use of the delayed coincidence technique is the ability to distinguish the prompt from the delayed curves as in Figure 7.33. That is, the time resolution must be smaller than the half-life. Typical time resolutions are of order 10 ns with Ge, 1 ns with NaI(Tl), and 0.1 ns with plastic scintillators. With careful measurement technique, the delayed coincidence method can be extended to half-lives below 10 ps, but its primary range of applicability is from 10^{-3} to 10^{-11} s.

For shorter half-lives, coincidence techniques are not applicable, and we must use a variety of other approaches. Some of these involve measuring the probability to excite a nuclear state by *absorbing* electromagnetic radiation from the ground state. Examples of such experiments will be considered in Sections 10.9 and 11.6. Other techniques are more applicable to nuclei produced in nuclear reactions. The product nuclei are allowed to recoil out of the reaction target; if

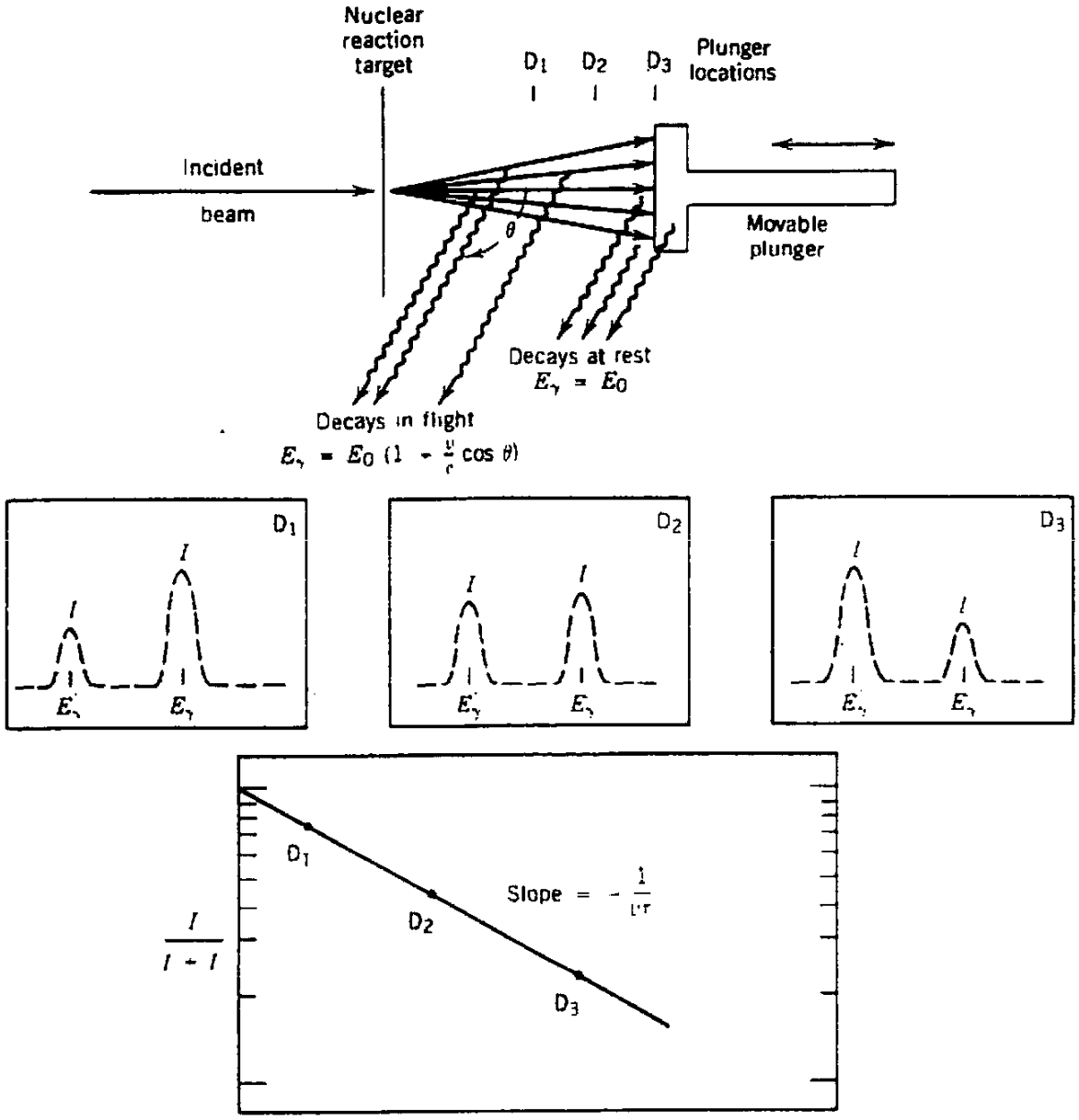

Figure 7.34 Schematic views of the Doppler-recoil method of lifetime measurement. Decaying nuclei are observed by a detector whose axis makes an angle θ with the recoil direction. Moving the plunger changes the relative numbers of decays in flight and at rest, which can be used to determine the mean life of the decay.

they are formed in an excited state, then the γ rays can be emitted while the nucleus is in flight. Such γ rays will be Doppler shifted. If the beam of recoiling nuclei is allowed then to be stopped (by striking a solid target), any remaining nuclei in the excited state will decay at rest and their energies will not be Doppler shifted. We therefore see two γ-ray peaks, one at the shifted energy and one at the unshifted energy. The relative intensities of the two peaks will depend on the distance through which the recoiling nuclei travel before stopping. (If the distance is short, fewer nuclei will decay in flight.) Figure 7.34 shows a schematic view of the experiment and its outcome. The fraction of γ rays in the unshifted peak shows an exponential dependence on the recoil distance, which in turn gives the half-life of the level. This method is useful in the range of 10^{-10} to 10^{-12} s. Below 10^{-12} s, the recoil distance will be so short that the technique cannot be easily used. (For a typical nonrelativistic nucleon, with $v = 0.1c$, the distance

traveled in 10^{-12} s is 0.03 mm.) Instead, the recoiling nucleus is allowed to penetrate a solid backing directly after the reaction. The nucleus immediately begins slowing down and eventually comes to rest; the velocity decreases continuously, and thus the γ emission varies continuously in energy from the shifted to the unshifted value. The profile of this energy distribution can be used to deduce the lifetime, once we understand the mechanism for energy loss by collisions

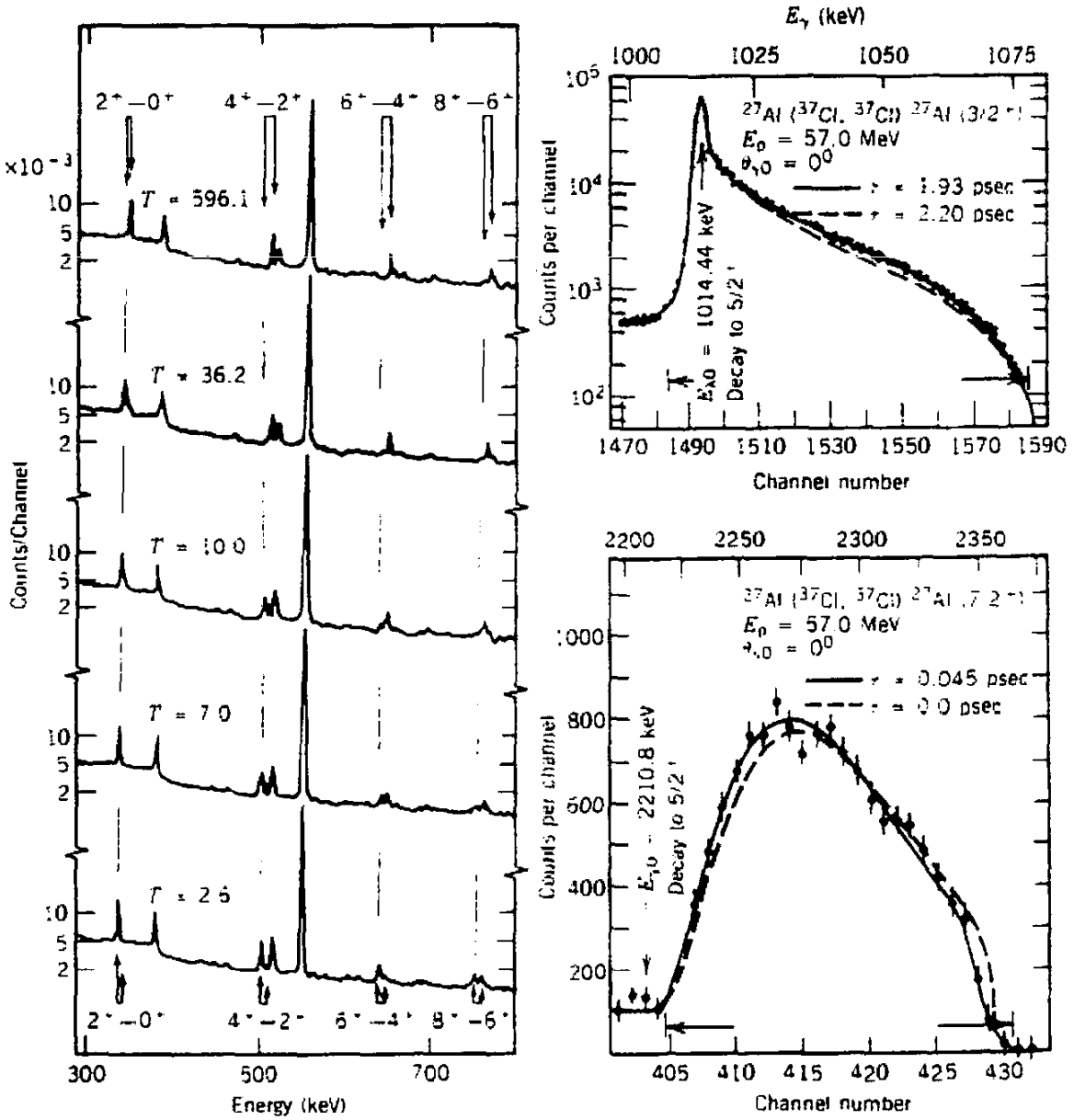

Figure 7.35 Doppler-shift methods for lifetime determination. At left are shown raw data for transitions in the ground-state rotational band (2^+, 4^+, 6^+, 8^+) of ^{122}Xe. The locations of the shifted and unshifted transitions are marked at the top and bottom. These data were taken with the detector at 0° in the geometry of Figure 7.34; thus the shifted line is at higher, rather than lower, energy. The various spectra were taken at plunger distances corresponding to flight times of 2.6 to 596.1 ps. The deduced half-lives are: $2^+ \rightarrow 0^+$, 61.9 ± 5.6 ps; $4^+ \rightarrow 2^+$, 5.7 ± 0.8 ps; $6^+ \rightarrow 4^+$, 2.7 ± 0.5 ps; $8^+ \rightarrow 6^+$, < 2.4 ps. At the right are shown two cases in which the lifetimes are so short that the recoil technique cannot be used. The line is broadened over the entire region from the shifted to the unshifted energy. The upper case yields a half-life of 1.33 ± 0.07 ps and the lower case gives 0.025 ± 0.013 ps. From W. Kutschera et al., *Phys. Rev. C* **5**, 1658 (1972); D. Schwalm et al., *Nucl. Phys. A* **293**, 425 (1977).

in the backing material. This technique is applicable down to about 10^{-15} s. Figure 7.35 shows applications of both techniques.

7.9 OTHER DETECTOR TYPES

Magnetic Spectrometers

In optical measurements, we use diffraction gratings to disperse light into its constituent wavelengths. We thus achieve a *spatial* separation of wavelength—different wavelengths appear at different locations, and can be recorded on a photographic film (as in a spectrograph) or recorded in intensity with a slit and a photoelectric device (as in a spectrometer). The goal in the design of an instrument to perform these measurements, as discussed in many introductory texts, is to achieve a high *resolving power* (defined as $\lambda/\Delta\lambda$, the ability to separate two nearby wavelengths at λ differing by $\Delta\lambda$) and a large *dispersion* (defined as $\Delta\theta/\Delta\lambda$, the angular separation $\Delta\theta$ per unit wavelength interval $\Delta\lambda$).

The goals in the design of magnetic spectrometers for charged particles are similar. We would like to have a device that has a large dispersion and a small resolution. (The definition of resolution is one of many areas of disagreement in terminology between atomic and nuclear physicists. The resolving power of a grating, $\lambda/\Delta\lambda$, should be a large number; the resolution of a nuclear radiation detector, $\Delta E/E$, should be as small as possible. These two statements are equivalent, but are stated in different terms. Both state that monochromatic radiation incident on the device should emerge with the smallest possible spread in energy or wavelength.) We would also like to have the highest possible efficiency: in the case of charged particles, we would like to be able to focus monoenergetic particles traveling in different directions to a common location on the output device.

The design of magnetic spectrometers shares many features with the design of mass spectrometers, which were discussed in Section 3.2 and illustrated in Figure 3.13.

The basic operation of all magnetic spectrometers is sufficiently similar that we will provide only the broad general details of operation and leave the discussion of design and construction to more detailed works. Figure 7.36 illustrates the basic principles. Let's assume the radioactive source emits two distinct radiations of energies E_1 and E_2 (α particles, for instance). These are of course emitted in many different directions. In the uniform magnetic field they follow circular trajectories in which the product Br determines the momentum of the particle (see Equation 3.20). Striking a recording device such as a photographic film, two distinct images are produced. All remaining details concern the design of the magnetic field to maximize the focusing effect and to improve the resolution.

A typical spectrometer for electrons is shown in Figure 7.37. The magnetic field is produced by a set of coils. For a particular value of the current in the coils (and thus of the field), electrons of one energy enter the output slit while others do not. A detector registers the electron intensity for different output currents. The resolution $\Delta E/E$ that can be obtained from such a device is typically below 0.1%, whereas the best resolution obtainable for electrons in a Si(Li) detector

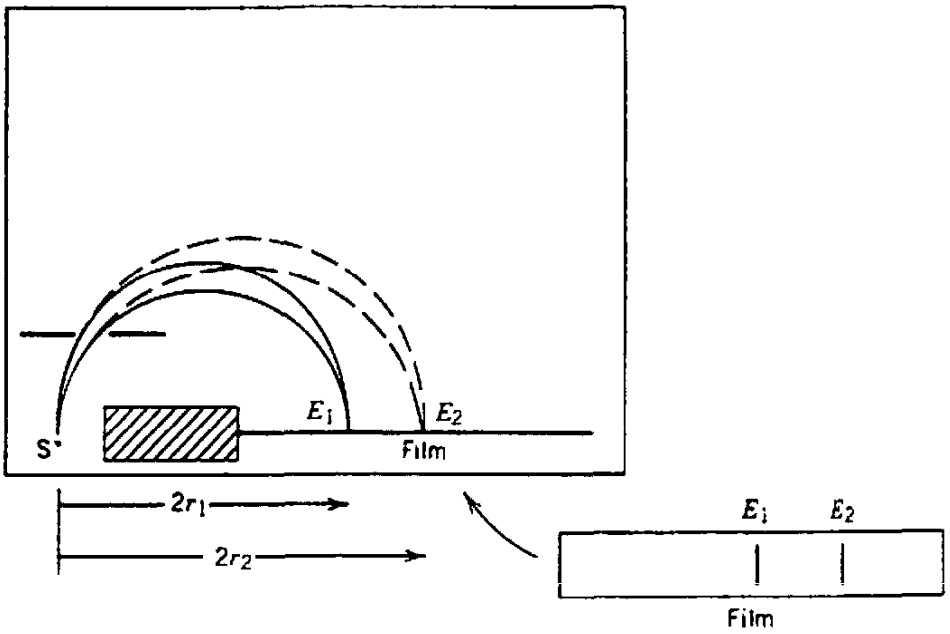

Figure 7.36 A simple magnetic spectrometer. There is a uniform magnetic field B perpendicular to the plane of the paper. The momentum of the particle determines the radius of curvature r of its path. There is also a focusing effect, as particles emitted in a narrow range of angles are focused to a common point on the film.

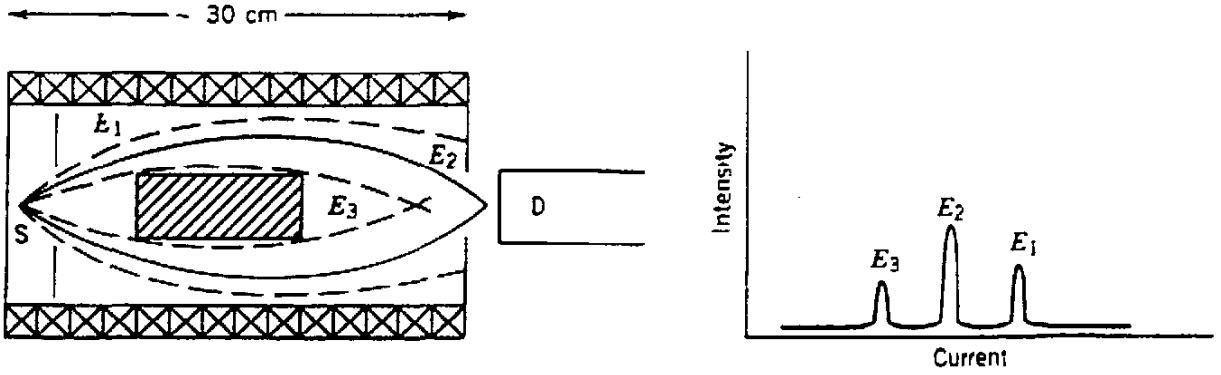

Figure 7.37 A magnetic "lens" spectrometer designed for electrons. The operation is very similar to that of an optical lens. The coils produce a magnetic field along the axis of the system. Particles of a unique energy E_2 are focussed on the exit slit and reach the detector; particles of different energies are not recorded. Changing the current in the coils allows different energy groups to be brought into focus and observed by the detector.

might be 0.5%. This improvement in resolution is often critical in studies of the intensities of internal conversion electrons from different subshells (see Section 10.6).

For heavy particles, such as alphas or protons, the design principles are similar but the construction must take into account the larger mass of the particles. Larger fields are required to bend the paths of these heavy particles, and generally this calls for designs using magnetic iron rather than current-carrying coils. The resulting radii of curvature are still large, and so the physical size of these devices is much larger than that of electron spectrometers. A typical size might be several meters, and the total weight of so much iron may be 100 metric tons! Figure 7.38 shows an example of a magnetic spectrometer designed for

Figure 7.38 High resolution proton spectrometer at the Los Alamos Meson Physics Facility. The incident proton beam enters through the pipe near the bottom left and scatters in the target chamber at the center. The scattered protons are deflected twice by the 75° vertical bending magnets and are detected at the top of the structure. The energy resolution is about 30 keV for 800-MeV protons. Photo courtesy Los Alamos National Laboratory.

heavy charged particles. The resolution is again about 0.1% or better, which is an improvement of a factor of 3–5 over Si(Li) or surface-barrier detectors.

Counter Telescopes

A counter telescope consists of two or more counters, in which the radiation to be observed passes in sequence through the counters and is usually totally absorbed in the last counter. Generally the last counter has the largest volume, in order to achieve complete absorption of the energy of the particle; the remaining counters in the telescope are very thin, so that the particle loses only a small amount of energy ΔE in each. The ΔE counters are usually chosen for their timing properties; plastic scintillators are the most popular choice, for they have

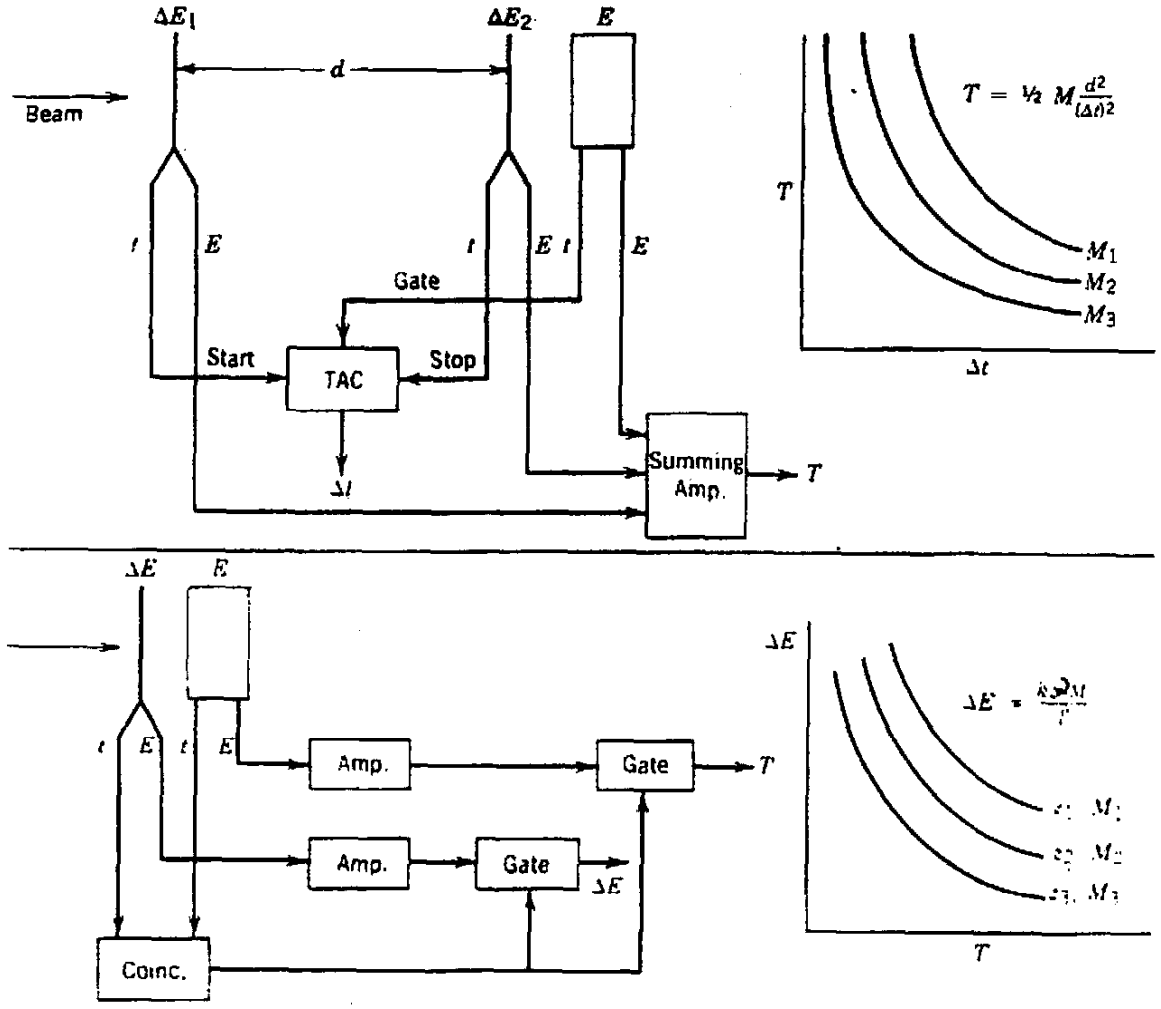

Figure 7.39 Two different examples of counter telescopes. (Top) In the time-of-flight technique, a TAC measures the time that it takes the particle to travel the distance d between the two ΔE detectors; a summing amplifier adds together the three energy losses to determine the energy of the particle. Plotting energy against Δt gives a family of hyperbolas that determine the mass of the particle. (Bottom) The $\Delta E \cdot T$ technique also gives a family of hyperbolas, which determine both z and M.

excellent timing and can be easily constructed in the variety of sizes and shapes needed for experiments. Other systems may use proportional counters, which can record the trajectory of the particle.

Counter telescopes have many different uses and can be constructed of a variety of different detectors. We consider only one application—their use as *particle identifiers*. (We discuss position-sensitive proportional counters in the next subsection.)

Figure 7.39 shows two simple telescopes that can be used for identifying particles. In the first method, we use two thin counters to extract timing signals; these timing signals can be used with a TAC to deduce the time that it took the particle to travel the distance between the two counters. We thus determine its velocity, and since its kinetic energy is determined from the E counter, we can deduce its mass. This technique is called the *time-of-flight* method and has applications other than particle identification; it is often used in measuring energies of neutrons, for which E counters do not give a photopeak and therefore give a relatively poor measure of the energy (see Chapter 12). Figure 7.40 shows a sample of the use of this technique to identify reaction products.

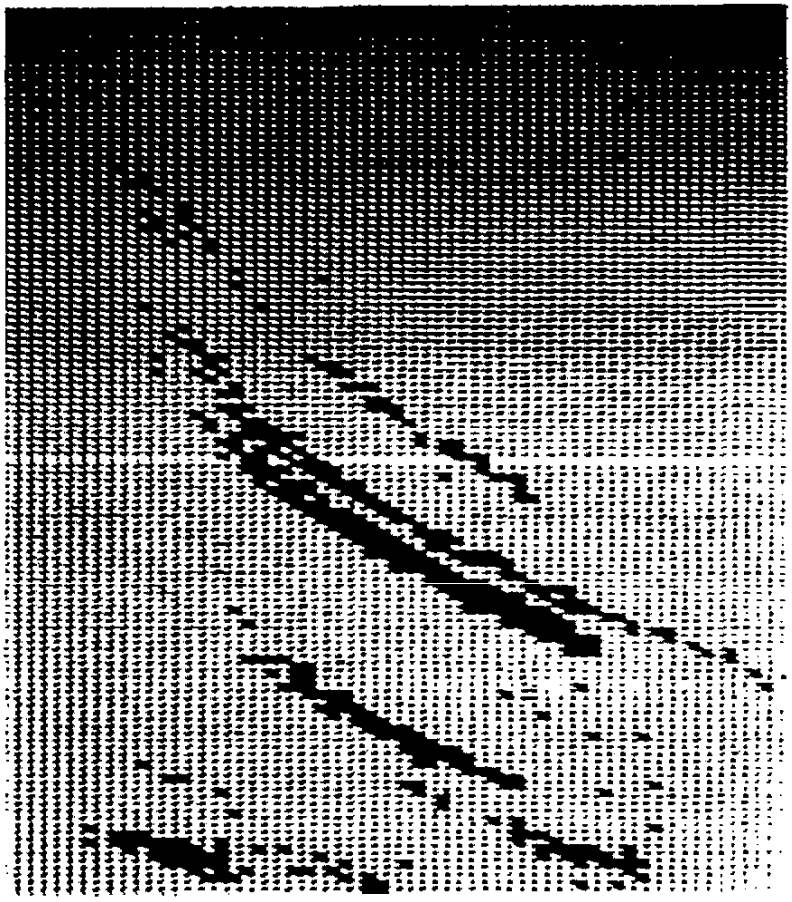

Figure 7.40 Time-of-flight particle identification. The data appear plotted as T against Δt, exactly as in Figure 7.39. From the top, the hyperbolas show ^{16}O, ^{13}C, ^{12}C, ^{7}Li, ^{6}Li, and ^{4}He. From W. F. W. Schneider et al., *Nucl. Instrum. Methods* **87**, 253 (1970).

The second technique involves the measurement of the energy loss in the thin counter. From the Bethe equation for stopping power, Equation 7.3, we see that $\Delta E \propto v^{-2}$ to a good approximation since the factors in the bracket will be small for nonrelativistic particles. Thus the product $\Delta E \cdot T$ is equal to kz^2M, where ze is the charge of the particle, M is its mass, and k is a constant (depending on the absorbing material). Graphing ΔE against T should yield a family of hyperbolas corresponding to the different values of z^2M. (Equation 7.7 for electrons can be written in a similar form for light relativistic particles.) Figure 7.41 shows the result of performing such a $\Delta E \cdot T$ analysis for a beam of particles.

Multiwire Proportional Counters

We include the multiwire proportional counter (MWPC) as an example of a detector that is sensitive to the position at which a particle interacts. We can use these detectors in a telescope arrangement to map the trajectory of a particle that results from a nuclear reaction. The basic MWPC (Figure 7.42) usually consists of two planes of individual anode and cathode wires, spaced perhaps 2–3 mm apart. The counter itself may be as large as 1 m^2. A charged particle passing through the chamber creates ionizing events that result in the avalanche occurring primarily in the vicinity of one of the wires. The wires are observed individually, and the output signals enable us to deduce the position of the particle within an uncertainty of the wire spacing (2–3 mm).

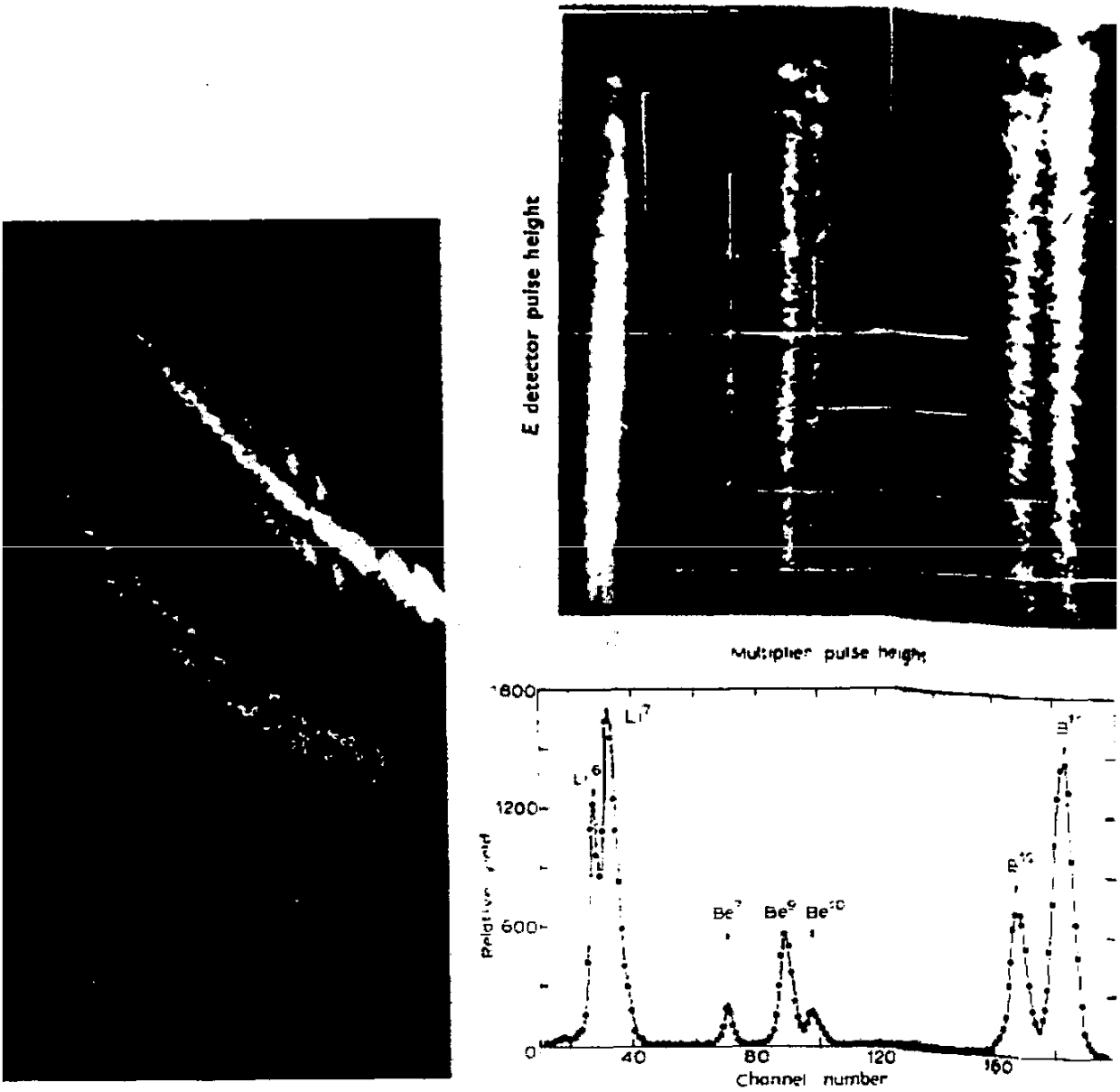

Figure 7.41 $\Delta E \cdot T$ method of particle identification. To the left is shown the hyperbola plots in the same form as in Figure 7.39. At the top right is shown data plotted in a slightly different format: T on the vertical scale and $\Delta E \cdot T$ on the horizontal scale. This way of plotting the data shows that $\Delta E \cdot T$ is indeed constant. At bottom right is shown the spectrum corresponding to the photograph; channel number gives the pulse height of the product $\Delta E \cdot T$. Notice that this method separates ^{7}Li from ^{7}Be and ^{10}Be from ^{10}B; these would not be separated in the time-of-flight technique, which is sensitive only to mass and not to charge. From M. W. Sachs et al., *Nucl. Instrum. Methods* **41**, 213 (1966).

Polarimeters

Often we wish to measure the polarization of the observed radiation. For spin-$\frac{1}{2}$ particles, such as electrons or nucleons, the polarization means the component of the spin (up or down) relative to a particular axis. For photons, we are usually interested in the classical linear polarization as determined by the $\mathbf{E}$ vector of the electromagnetic radiation field.

The Compton scattering of photons is dependent on polarization, as shown in Figure 7.43. If we observe the intensity of the scattered radiation at different positions about the scatterer, we can deduce the degree of linear polarization of the incident radiation. A second method, used most often for measurement of

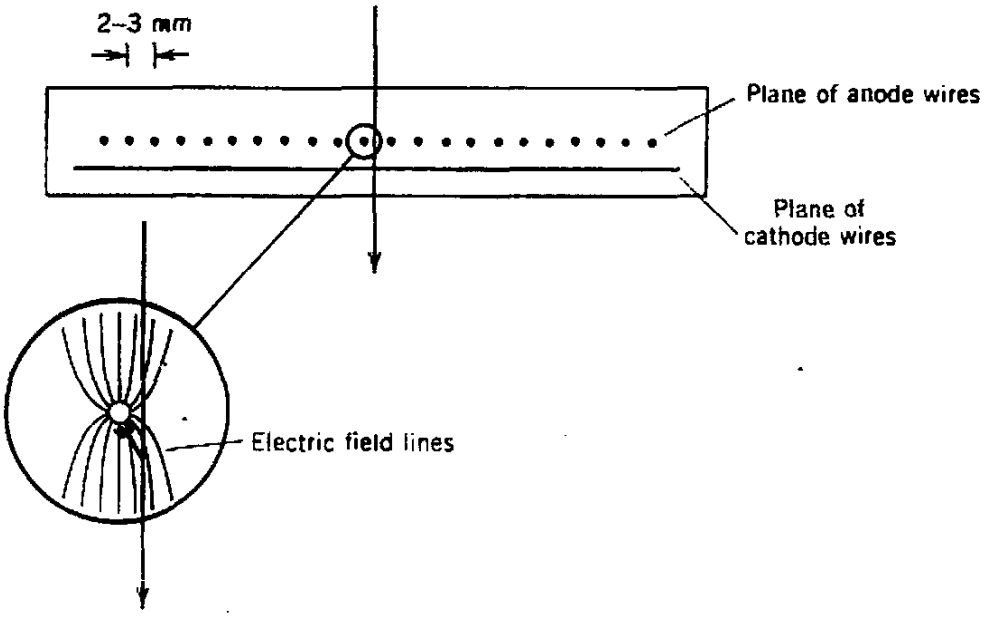

Figure 7.42 Schematic view of multiwire proportional counter. The passage of a charged particle near one of the anode wires causes an avalanche that is read out as a signal on that wire only. The particle can thus be located to within an uncertainty of the wire spacing. The wires and the entrance and exit windows are extremely thin, so that the particle loses very little energy. These detectors are usually operated in a telescope with a thick *E* counter at the end to determine the energy of the particle.

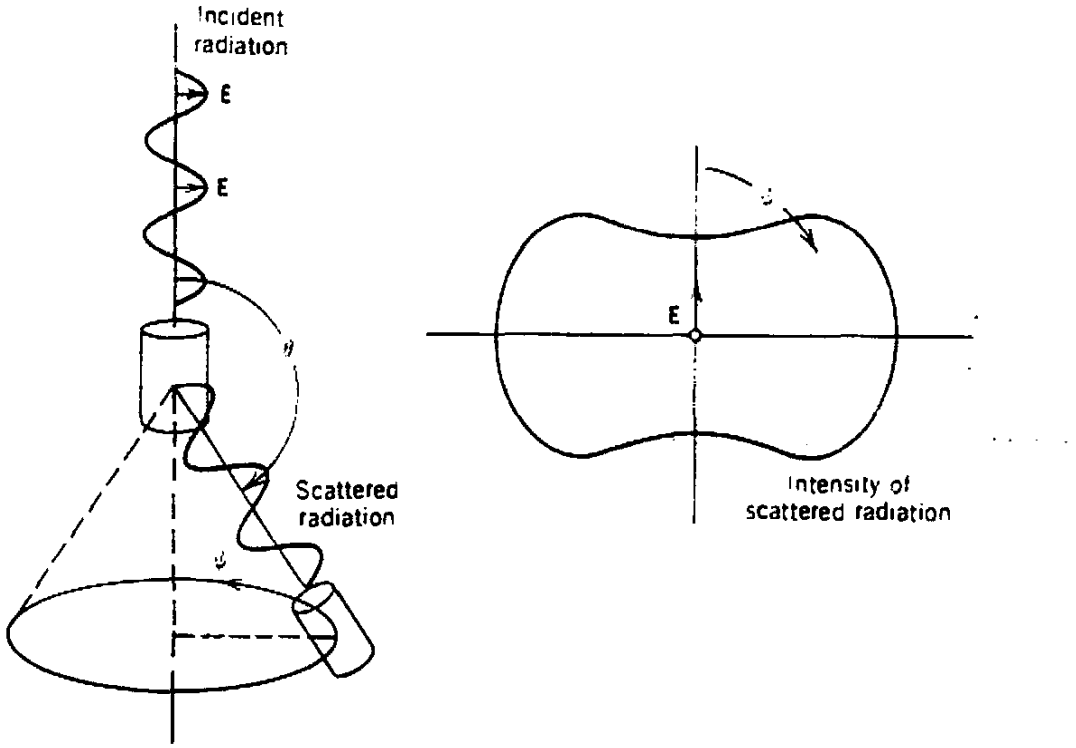

Figure 7.43 A Compton polarimeter. As the detector travels in the cylindrical geometry over various values of ψ, the scattered intensity varies because of the polarization dependence of the Compton-scattering process. Measuring the intensity of the scattered radiation at two or more angles ψ will enable the plane of polarization (direction of E) to be deduced.

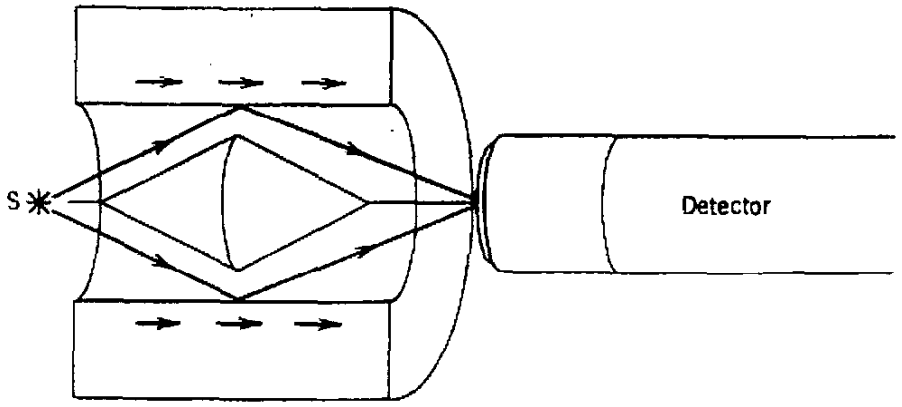

Figure 7.44 The Compton-scattering process also depends on the polarization of the electrons of the scattering material. Here the scattering material is magnetized iron. Reversing the direction of magnetization (by reversing the current in an electromagnet) will cause a change in the intensity of the radiation observed by the detector, from which the circular polarization can be deduced.

circular polarization, is based on the probability of scattering of photons from polarized electrons such as in a magnetic material. From the difference in intensity of the scattered radiation when the field is reversed, we can deduce the polarization (Figure 7.44).

Measuring the polarization of spin-$\frac{1}{2}$ particles also involves doing a scattering experiment. It is well known that the scattering of polarized electrons from polarized electrons (again, as in magnetic material) depends strongly on whether the spins of the electrons are parallel or antiparallel. The Pauli principle inhibits scattering in the parallel configuration, and thus scattering in the antiparallel arrangement is strongly preferred. (The ratio of cross sections for parallel and antiparallel scattering is in the range 0 to 0.1 at low energies.) For positron-electron scattering, the Pauli principle does not apply and the cross sections become equal at low energy.

Polarimeters for nucleons depend on the spin dependence of nuclear scattering, which was discussed in Chapter 4. Here we do not need to scatter from spins that are themselves polarized (as we did with electrons, for instance). The nuclear spin-orbit interaction gives the scattering cross section its spin dependence, and it is perfectly acceptable to determine polarizations by scattering of neutrons or protons by a spinless target such as ^{4}He. Generally we use this technique to analyze the polarization of the products of nuclear reactions, which we discuss in Chapter 11.

REFERENCES FOR ADDITIONAL READING

For comprehensive and up-to-date references on nuclear radiation detectors, see Glenn F. Knoll, *Radiation Detection and Measurement* (New York: Wiley, 1979), and J. B. A. England, *Techniques in Nuclear Structure Physics* (New York: Wiley, 1974). These two works contain extensive references to the original literature, and the latter work has a particularly good review of magnetic spectrometers.

Other general texts and references on this topic include G. G. Eichholz and J. S. Poston, *Principles of Nuclear Radiation Detection* (London: Butterworths, 1980); R. E. Lapp and H. L. Andrews, *Nuclear Radiation Physics*, 4th ed.

(Englewood Cliffs, NJ: Prentice-Hall, 1972); P. W. Nicholson, *Nuclear Electronics* (London: Wiley, 1974); R. D. Evans, *The Atomic Nucleus* (New York: McGraw-Hill, 1955). Chapters 18–25; G. Dearnaley and D. C. Northrop, *Semiconductor Counters for Nuclear Radiations* (New York: Barnes and Noble, 1966); J. R. Birks, *The Theory and Practice of Scintillation Counting* (New York: MacMillan, 1964).

Many topics concerning detectors, electronics, and techniques are covered in *Alpha-, Beta-, and Gamma-Ray Spectroscopy*, edited by K. Siegbahn (Amsterdam: North-Holland, 1965). See especially Chapters 1 and 2 on interactions of radiation with matter, Chapter 3 on spectrometers, Chapter 5 on scintillators, Chapter 6 on particle detectors, Chapters 7 and 8 on general experimental techniques, and Chapter 17 on measuring short lifetimes.

Photon cross sections are tabulated in E. Storm and H. I. Israel, *Nuclear Data Tables A* 7, 565 (1970). Electron ranges in matter can be found in L. Pages, E. Bertel, H. Joffre, and L. Sklavenitis, *Atomic Data* 4, 1 (1972).

For reviews of techniques for measuring nuclear lifetimes, see A. Z. Schwarzschild and E. K. Warburton, *Ann. Rev. Nucl. Sci.* **18**, 265 (1968). Techniques of particle identification are reviewed by F. S Goulding and B. G Harvey, *Ann. Rev. Nucl. Sci.* **25**, 167 (1975).

PROBLEMS

1. Use the ranges given in Figure 7.2 to compute the range of (a) a 10-MeV α particle in gold; (b) a 5-MeV proton in beryllium; (c) a 1-MeV proton in water. Express the range in centimeters.
2. Find the range (in centimeters) in aluminum of 4.0-MeV ^{3}He and ^{3}H.
3. Calculate the energy loss ΔT of protons, deuterons, and α's between 10 and 200 MeV in passing through a 2-mm thickness of solid plastic scintillator. Plot ΔT against T.
4. Calculate and sketch the range of protons in NaI for energies between 1 and 100 MeV. (Extrapolate as necessary from Figure 7.2.)
5. The immediate environment of an accelerator or reactor contains large fluxes of γ rays of energies in the vicinity of 5–10 MeV. What thickness of lead is required to reduce the photon intensity by a factor of 10^{12}?
6. An α-particle point source of 25 μCi is placed in contact with one face of a large ionization chamber. The source emits a single α particle of energy 6.20 MeV. If the α particles that enter the chamber lose all their energy in the chamber, what is the current produced at the output of the chamber? (Assume 100% efficiency for collecting the charges in the chamber.)
7. A Geiger counter used in several applications over the course of a typical day produces on the average 100 counts per second. The tube is in the form of a cylinder 2 cm in diameter by 10 cm long and is filled with a mixture of 90% argon and 10% ethanol to a pressure of 0.1 atmosphere. In the Geiger-Müller region, each output count results from the formation of about 10^{10} ion-electron pairs. How long will it take for one-third of the quenching gas to be used up, thus necessitating replacement of the tube?

8. The pulse-height spectrum of a radioactive source, known to emit only monoenergetic photons of fairly high energy, shows three prominent peaks, at pulse heights of 7.38, 6.49, and 5.60 V. What is the γ-ray energy?
9. The 662-keV photon in the decay of ^{137}Cs is observed by a NaI detector with an energy resolution (FWHM) of 53 keV. What will be the resolution for a measurement of the 1.836-MeV photon in the decay of ^{88}Y?
10. Find the energy of the Compton edges in a γ-ray spectrum of the decay of ^{60}Co (see Table 7.2).
11. In the decay of ^{88}Y, two photons are emitted with energies of 0.898 MeV (92% of decays) and 1.836 MeV (100% of decays). Sketch the expected γ-ray spectrum, as in Figure 7.26, when a source of ^{88}Y is placed in front of a NaI detector and a Ge detector.
12. For the binomial, Poisson, and Gaussian distributions, derive the expressions for the variance σ^2.
13. A certain radioactive source gives 3861 counts in a 10-min counting period. When the source is removed, the background alone gives 2648 counts in 30 min. Determine the net source counting rate (counts per second) and its uncertainty.
14. A technician is given the job of determining the strength of a radioactive source to the greatest possible precision. The counting equipment is in great demand, and only 1 h of total measuring time is available. How should the available time be scheduled if: (a) the net source counting rate is about 5 times the background rate; (b) the net source counting rate is about equal to the background rate; (c) the net source counting rate is about one-fifth of the background rate?
15. A coincidence counting experiment consists of two γ-ray detectors; one is fixed at a position defined as $\theta = 0^\circ$ and the other can move in a horizontal plane to various values of θ. The source, located on the axis of rotation of the second detector and equidistant from the two detectors, emits a γ ray of energy 750 keV. It is possible for the photon to enter one detector and produce a single Compton-scattering event, following which the scattered photon can then travel to the other detector to be absorbed. Plot the energy of the radiation observed in the moveable detector against its position when this scattering occurs. (*Note*: In this geometry, θ is *not* the Compton-scattering angle.)
16. The thickness of a metallic foil is regulated during the manufacture by observing the attenuation of a beam of photons passing through the foil. A source of photons is placed above the foil as it emerges from the rollers, and a detector is placed below the foil. The photon energy is chosen so that the attenuation is exactly 50% at the desired thickness of 0.10 mm. The detection efficiency with no foil in place is 1%. To regulate the rollers, it is necessary to make a determination of the thickness in at most 1 s, and the thickness must be regulated to $\pm 5\%$. Calculate the required source strength.
17. What would be the appearance of a time-to-amplitude spectrum (such as Figure 7.32) if the two radiations were so close in energy that the detectors were unable to distinguish between them?